
Article:
Blitz, MA orcid.org/0000-0001-6710-4021, Pilling, MJ, Robertson, SH et al. (2 more authors) (2021) Global Master Equation Analysis of Rate Data for the Reaction C2H4 + H ⇄ C2H5: ΔfH0⊖C2H5. The Journal of Physical Chemistry A. acs.jpca.1c05911. ISSN 1089-5639

https://doi.org/10.1021/acs.jpca.1c05911

A Global Master Equation Analysis of Rate Data for the Reaction $C_2H_4 + H \rightleftarrows C_2H_5$: $\Delta_f H_0^{\ominus} C_2H_5$

Mark A. Blitz[1,2,*], Michael J. Pilling[1], Struan H. Robertson[3,*], Paul W. Seakins[1,*] and Thomas H. Speak[1]

1. School of Chemistry, University of Leeds, Leeds, LS2 9JT, UK

2. National Centre for Atmospheric Science (NCAS), University of Leeds, Leeds, LS2 9JT, UK

3. Dassault Systèmes, 334 Science Park, Cambridge, CB4 0WN

Abstract

While forward and reverse rate constants are frequently used to determine enthalpies of reaction and formation, this process is more difficult for pressure dependent association/ dissociation reactions, especially since the forward and reverse reactions are usually studied at very different temperatures. The problems can be overcome by using a data-fitting procedure based on a master equation model. This approach has been applied to existing experimental pressure dependent forward and reverse rate coefficients for the reaction $C_2H_4 + H \rightleftarrows C_2H_5$ (k_1, k_{-1}) using the MESMER code to determine $\Delta_f H_0^{\ominus} C_2H_5$ from the enthalpy of reaction. New measurements of k_1, k_{-1} were included in the analysis. They are based on laser flash photolysis with direct observation of H atom time profiles by VUV laser induced fluorescence under conditions where the approach to equilibrium could be observed. Measurements were made over the temperature range 798 – 828 K and with [He] from 2.33 – 7.21 x 10^{18} molecule cm^{-3}. These data were then combined with a wide range of existing experimental data with helium as the bath gas (112 measurements of k_1 and k_{-1}, covering the temperature range 285 – 1094 K and [He] = 7.1 x 10^{15} – 1.9 x 10^{19} molecule cm^{-3}) and fitted using the master equation solver MESMER. The required vibrational frequencies and rotational constants of the system were obtained from *ab initio* calculations and the activation threshold for association (ΔE_{thresh}), enthalpy of reaction ($\Delta_r H_0^{\ominus}$), imaginary frequency (υ_{imag}) and helium energy transfer parameters ($\langle \Delta E \rangle_{d,298} (\frac{T}{298})^n$) were optimized. The resulting parameters (errors are 2σ) are ΔE_{thresh}=11.43 ± 0.34 kJ mol^{-1}, $\Delta_r H_0^{\ominus}$ = -145.34 ± 0.60 kJ mol^{-1}, υ_{imag} = 730 ± 130 cm^{-1}, $\langle \Delta E \rangle_{d,298}$ = 54.2 ± 7.6 cm^{-1}, *n* = 1.17 ± 0.12. A value of $\Delta_f H_{298.15}^{\ominus}$ (C_2H_5) = 120.49 ± 0.57 kJ mol^{-1} is obtained by combining $\Delta_r H_0^{\ominus}$ with standard enthalpies of formation for H and C_2H_4 and making the appropriate temperature corrections. The dependence of these parameters on how the internal rotor and CH_2 inversion modes are treated has been explored. The experimental data for other bath gases have been analysed and datasets compatible with the potential energy surface parameters determined above have been identified. The parameters are virtually identical, but with slightly smaller error limits. Parameterization of k_1, k_{-1} using the Troe formalization has been used to investigate competition between ethyl decomposition and reaction with oxygen under combustion conditions.

1. Introduction

The availability of accurate enthalpies of formation for alkyl radicals has been substantially enhanced by the development of the Active Thermochemical Tables (ATcT) [1-2]. Theory has played a key role in contributing to ATcT and also in providing a test of its accuracy [3]. The current version of ATcT gives $\Delta_f H_0^{\ominus}$ = 131.04 ± 0.27 kJ mol^{-1} for the ethyl radical. One advantage of the ATcT compilation is that it is based on extensive thermochemical networks of data, with wide-ranging provenance, providing robust results of high accuracy. In the case of the ethyl radical, there are over 450 contributors to 90% and 20 contributors to 31% of the provenance. The top contributors are based on ionization energies [4-5] and the measurement of forward and reverse rate coefficients for the reaction:[6-9]

$$C_2H_5 + HBr \rightleftarrows C_2H_6 + Br$$

The association and its reverse dissociation reaction

$$C_2H_4 + H \rightleftarrows C_2H_5 \qquad \text{(R1)}$$

have been used to determine $\Delta_f H_0^{\ominus}$ (C_2H_5) through the measurement of the bimolecular forward (k_1) and reverse, unimolecular (k_{-1}) rate coefficients from the approach to equilibrium at T ~ 800 K [10-11]. The uncertainties in the enthalpy of formation that result, coupled with the limited range of temperature over which the technique could be used, resulted in a limited contribution to the ATcT result. The temperature range could be extended by calculating the equilibrium constant from forward and reverse rate coefficients under irreversible conditions. This is difficult, though, because of the pressure dependence of the reaction and the large temperature differences of conditions used to study the association (200 – 600 K) and dissociation reactions (800 – 1000 K). This temperature range, of course, becomes an advantage if a method can be used that analyses the whole set of forward and reverse rate data globally, and accommodates the pressure dependence of the reaction rates.

Association / dissociation reactions and their pressure dependence can be modelled using a master equation approach.[12-14] The master equation solver MESMER[12] uses a matrix technique to determine the rate coefficients. As discussed in more detail below, MESMER has the facility to vary a number of parameters to fit a large set of experimental rate data to the modelled rate coefficients. This technique has been used to model and parameterize rate coefficients and thermodynamic data for the reversible reactions peroxy radicals + NO_2 [15] and OH + C_2H_4.[16] The ethyl radical system produces additional challenges because the experimental database is very extensive and covers a wide range of temperatures and a number of bath gases.

The approach works best if the number of variable parameters is kept to a minimum. One approach is to combine the ME modelling / fitting with electronic structure calculations so that the microcanonical rate coefficients in the model have some degree of constraint. In addition, ethyl has two low frequency modes, which play a crucial role in calculating the densities of states which are central to the ME model. Calculations of the potential energy surface (PES) are essential in assessing the representation of these modes and their contribution to the densities of states.

Energy transfer parameters are also important in the calculations and are used as variable parameters. The wide range of conditions used for some of the third bodies in the experimental studies allows, in principle, good definition of the energy transfer parameters for these species. Feng et al.[17], who studied ethyl dissociation (k_{-1}) at low pressures, found significant differences between the energy transfer parameters returned from modelling their results and from modelling the results from Brouard et al.[10] and Hanning-Lee et al.[11] who studied forward and reverse reactions, under equilibration conditions, but at higher pressures than those used by Feng et al.[17]

In this paper we present new experimental results (Section 2) to address the issue outlined in the last paragraph. The data were obtained by the direct observation of the approach to equilibrium of R1 at temperatures of ~800 K. In Section 3 we discuss the methods used to calculate the PES parameters and present the *ab initio* PES for R1. Particular emphasis is given to the low frequency modes, the torsion of CH_3 and the inversion of CH_2. A good deal of attention is paid to the calculation of the densities of states because of their importance in the final determination of $\Delta_f H_0^{\ominus}(C_2H_5)$. The new experimental data were combined with literature data, which cover a very wide range of temperature, pressure, bath gases and experimental techniques, and a master equation based fitting exercise has been performed to determine the PES parameters to compare with our *ab initio* calculations and other results. A comprehensive model is required to analyse systematically the wealth of experimental data available. Section 4 provides a brief discussion of the master equation fitting methodology using MESMER and the approach to global fitting of the experimental data. The results and implications of the fitting are presented in in Section 5 and final conclusions are drawn in Section 6.

2. Experimental Study of the $\mathbf{C_2H_4 + H \rightleftarrows C_2H_5}$ Approach to Equilibrium

2.1 Experimental Method

The H + C_2H_4 reaction was studied using a conventional slow-flow, laser flash photolysis/laser induced fluorescence (LIF) apparatus with helium as the bath gas.[18-21] H atoms were generated by pulsed laser photolysis of ethene or ammonia and their removal in an excess of ethene was monitored by VUV laser induced fluorescence. Experiments were carried out in a slow-flow, stainless steel, multiport reaction cell, which was surrounded by a custom-made ceramic fibre heater (Watlow) that allowed temperatures to be set in excess of 850 K. Two thermocouples were mounted in the centre of the cell. Two sets of ports on the horizontal axis were used to couple in and out the photolysis and probe beams. Other ports on the reaction cell allowed gases to be flowed into and out of the cell and the pressure recorded via a Baratron pressure gauge (1000 Torr, MKS).

The photolysis-axis port windows were quartz and allowed the 193 nm light from the photolysis laser (Lambda Physik LPX100) to enter and exit the cell. H atoms were mainly produced from NH_3 (~ 10^{13} molecule cm^{-3}) but were also produced from C_2H_4 when its concentration was high, $C_2H_4 \leq 10^{15}$ molecule cm^{-3}:

$$NH_3 \xrightarrow{193\ nm} NH_2 + H \qquad \text{P1}$$

$$C_2H_4 \xrightarrow{193\ nm} C_2H_3 + H \qquad P2$$

This laser energy was typically a few mJ / pulse (~10^{15} photons) and in a few experiments the NH_3 193 nm cross-section was measured using an energy meter (JMAX) located beyond the exit port; the cross-section was in agreement with the literature [22]. Typical initial H atom concentrations were a few 10^{11} atom cm^{-3}, although some experiments were performed at higher concentrations where absorption, as well as LIF, could be observed.

The H-atom probe laser was at right-angles and in the same plane as the photolysis laser. This axis had MgF_2 port windows that allowed the 121.56 nm light (Lyman-α) to traverse this axis and overlap (~2.5 cm) the photolysis light in the centre of the cell. The vacuum ultraviolet (VUV) light was generated by frequency tripling using a Kr:Ar mixture (~1:2.5) in a glass cell, where the front window was MgF_2 and was located close to probe port window; the gap between the tripling cell and reaction cell was purged with N_2. A dye laser (Sirah, Cobra Stretch) pumped by a 532 nm YAG laser (Continuum Powerlite 8010) was used to generate light at ~ 729.36 nm (Pyridine 2). This light was doubled to produce 10 – 15 mJ / pulse of 364.68 nm light that was focused (15 cm lens) into the tripling cell. The pressure of the Kr:Ar mixture was typically a little above atmospheric pressure in order to maximize the tripling process. [23] This probe beam exited the cell into a purged tube (N_2) that allowed the probe laser light to reach a quartz flat mount at 45° so that the VUV was reflected through a VUV interference filter (Acton Research) and onto a solar blind photomultiplier (Thorn EMI); the light recorded by this PMT (via an oscilloscope LeCroy, Waverunner LT 262) monitored the pulse-to-pulse stability of the light and was also used to monitor the H atom in absorption and to optimise the Kr:Ar mixture for maximum VUV output.

At high [C_2H_4], significant [H] was generated from P1, where up to ~ 20% absorption was observed via the PMT signal. This implies that [H] was equal to ~ 6×10^{11} molecule, based on a photolysis path length of 2.5 cm and $\sigma_{Lyman\text{-}\alpha,\ 800\ K} = 1.6 \times 10^{-13}$ cm^2 (from Okabe[24] and adjusted for the Doppler width at 800 K). The absorption PMT also recorded the attenuation of the VUV light by the C_2H_4 over the whole length of the reaction cell, 27 cm. As the optical path distances in the reaction cell to the LIF and absorption PMTs were equal, the LIF signal was corrected for absorption by simply dividing the LIF signal by the transmitted radiation and used in the kinetic analysis.

To collect the fluorescence internal MgF_2 lenses imaged the vacuum-ultra-violet fluorescence through an MgF_2 port window onto the solar blind channel photomultiplier (Perkin-Elmer, CPM 911). Both signals (LIF and absorption) from the oscilloscope were boxcar integrated and then passed to the PC for storage. A delay generator (BNC 555) scanned the time delay between the photolysis and probe lasers and built-up the H atom time profiles. A LabVIEW program was used to control the firing of the delay generator and display of the H atom signals from the oscilloscope. The repetition rate of the lasers was 2 Hz.

Helium (BOC CP grade, 99.999%) and ethene (Aldrich, ≥ 99.5%) were used from the cylinders without purification. NH_3 (BOC) was freeze-pumped thawed before being diluted in helium in a glass bulb. These gases were flowed to the reaction cell using calibrated mass flow controllers (MKS), where the total flow was ~ 500 and 1500 SCCM for 200 and 600 Torr experiments, i.e. the residence time in the reaction cell was approximately constant. A needle valve located between the rotary pump and the cell was used to control the cell pressure. The gas flow was perpendicular to the plane

of the photolysis and probe lasers. At a photolysis repetition rate of 2 Hz, this flow was sufficient to ensure that each laser pulse interrogated a fresh sample of gas. Tests were carried out to ensure there was no dependence of the kinetics on flow rate at a fixed pressure.

2.2 Experimental Results

These experiments were specifically focused on the reaction between H atoms and ethene at temperatures where equilibrium is observed:

$$C_2H_4 + H \rightleftarrows C_2H_5 \qquad \text{R1}$$

Under these conditions, the enthalpy change of reaction sensitively influences the kinetics. Examples of this equilibrium behavior can be seen in frames 1 - 4 of Figure 1.

All the data at a given temperature and pressure, ~10 traces with [C_2H_4] varied in the range 0 – 9.41 × 10^{14} molecule cm^{-3}, were fitted simultaneously in a global analysis using Origin, where an analytical equation (see Supplementary Information (SI) Section 1) was used to describe the kinetic scheme. (In our previous work on the OH + C_2H_4 system[16] we used a direct trace analysis approach where experimental traces were compared directly with those generated from a master equation. Ideally, the same approach would be used here; however, as described below, the results from these experiments were combined with existing results from other workers and so a more conventional approach to the analysis of the data was employed.) The scheme includes k_1 and k_{-1} from R1, and also recognizes that both H and C_2H_5 can be lost from the system. For H atoms this will be a combination of diffusion (approximately first order) and reaction with the ammonia precursor (pseudo first order) and this rate coefficient, k_{1st}, was measured independently for each set of conditions. C_2H_5 will be lost predominantly via diffusion:

$$H \xrightarrow{k_{1st}} \text{loss}$$

$$C_2H_5 \xrightarrow{k_{C2H5,diff}} \text{loss}$$

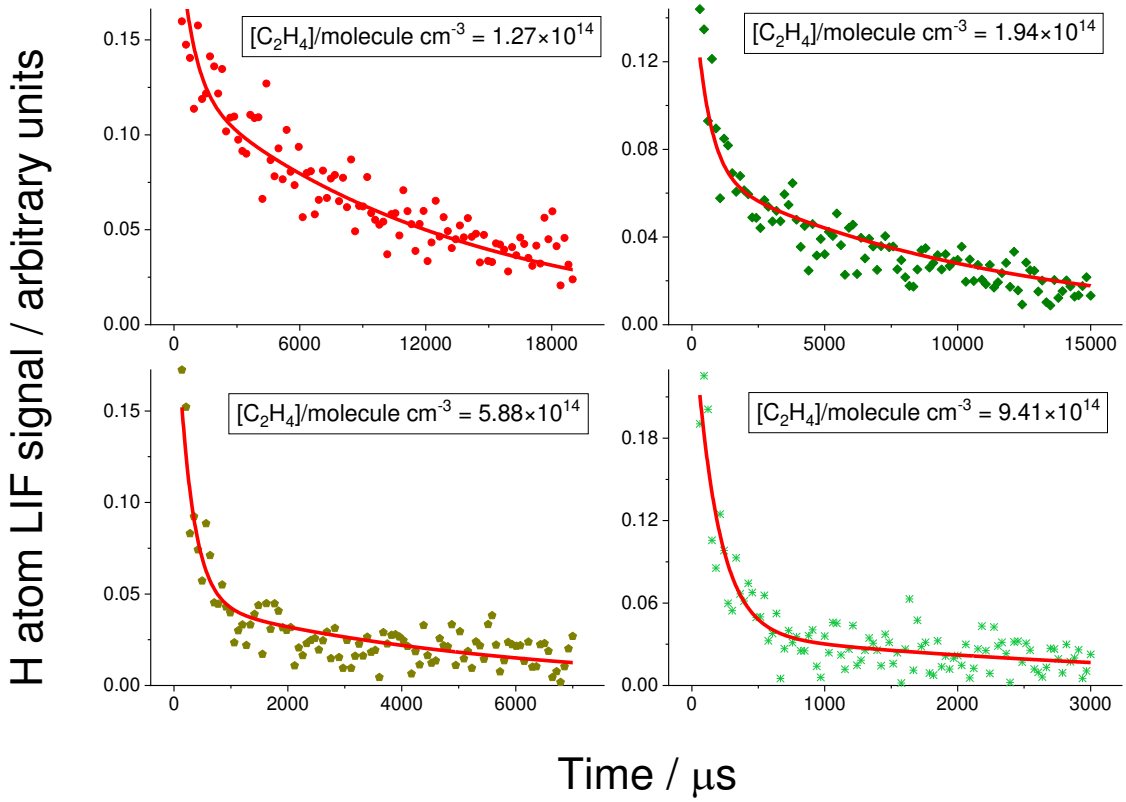

Figure 1. Examples of experimental data of H atom traces ranging from approximately single-exponential H decay to strongly bi-exponential, equilibration behavior. Data were recorded at 828 K, [He] = 6.71× 10^{18} molecule cm^{-3} and with a total flow rate of 1439 sccm. [C_2H_4] ranged from 0 – 9.41 × 10^{14} molecule cm^{-3}.

In addition, there was evidence that, at the highest ethene concentration, C_2H_5 reacted with the vinyl radical, C_2H_3, produced from ethene photolysis. Despite the low vinyl concentration, this reaction competes because of its high rate coefficient ~ 10^{-10} cm^3 $molecule^{-1}$ s^{-1}.[25] In order to retain an analytic expression for $[H]_t$, this reaction was approximately accommodated in the kinetic scheme as a reaction that scales with ethene concentration:

$$C_2H_5 \xrightarrow{k_2} \text{loss} \qquad\qquad k_2[C_2H_4]$$

The analytical equation for this scheme, involving k_1, k_{-1} k_{1st} and $k_{diff,C2H5}$ and k_2, is given in the SI (Section 2), and Figure 1 includes examples of the fit to the data. Ignoring k_2 reduces k_1 by ~ 5%, which is consistent with k_1 being about 20 times larger than k_2; H atoms also react with C_2H_3 with a similar rate coefficient as k_2, so the reported k_1 might require ~ 5% reduction, but this is close to the reported errors, see Table 1 (with further details in Table S1). The returned parameters are also independent of the flow rate as would be expected as each photolysis pulse interacts with a fresh portion of gas as the flow is perpendicular to the plane of the photolysis and probe lasers. The resulting values of the reaction 1 parameters from this analysis are given in Table 1.

Table 1. Results of the global analysis of the experimental traces for the $C_2H_4 + H \rightleftarrows C_2H_5$ equilibration. The errors represent 2 standard deviations (2σ).

T / K	[He] / cm^{-3}	k_1 / molecule cm^{-3} s^{-1}	k_{-1} / s^{-1}	Total flow / SCCM	Traces
798	2.33×10^{18}	$2.84 \pm 0.11 \times 10^{-12}$	141 ± 26	494	9
796	7.20×10^{18}	$4.53 \pm 0.25 \times 10^{-12}$	241 ± 55	1439	12
828	6.71×10^{18}	$5.18 \pm 0.14 \times 10^{-12}$	712 ± 35	1439	15

As mentioned in the introduction, the reason for including additional experimental evidence was to check on the discrepancy between the energy transfer parameters of the earlier work by Pilling and co-workers [10-11] and Feng et al. [17] The current data are better constrained than earlier studies; using LIF gives better sensitivity than the earlier resonance fluorescence measurements and, at higher [H], detection by both LIF and absorption data can be used. The use of ammonia as the H atom source provides an independent means of varying $[H]_0$ and $[C_2H_4]$. The earlier studies used ethene photolysis to generate H; more significant corrections were needed in the earlier work for radical – radical reactions, involving extrapolations to zero radical concentrations.

Our preliminary analysis suggests that the current results are in good agreement with the earlier work of Pilling and co-workers (see Section 5). For the present, we include our current experimental work as an additional dataset in the global analysis (Section 4) and return to the discrepancy in energy transfer parameters identified by Feng et al. in Section 5.3.3.

3. Modelling

The master equation (ME) has been discussed at length in many other places (e.g. see Robertson[26] and Miller et al.[27]) and the implementation used in the current analysis, MESMER, can be found in Glowacki et al.[12], so details of the solution of the ME will not be given here, except to say that all fitting was done using a one dimensional ME for largely practical reasons resulting from the large number of iterations needed in fitting to experimental data. Given the near barrierless association of the forward reaction it is possible that effects due to angular momentum are important as Miller and Klippenstein[28] suggest, but the diagonalization of a two dimensional collision operator is substantially more expensive and so was not implemented. However, following a short discussion of the *ab initio* calculations, the determination of the density of states, which are critical for an accurate fit of the data, is discussed in detail.

3.1 *Ab initio* Calculations

Geometry optimizations of all the species involved in the title reaction were performed with the DFT method M06-2X, along with the post–Hartree–Fock methods coupled-cluster with single and double excitations (CCSD) and quadratic configuration interaction (QCISD) with the augmented Dunning type triple zeta correlation consistent basis set, aug-cc-pvtz (ATZ), with Gaussian 09.[29] Harmonic frequencies were corrected for higher order PES expansion terms around the equilibrium

position. For CCSD and QCISD this was done using average frequency scaling factors taken from the Computational Chemistry Comparison Benchmark Database (CCCBD).[30] For structures calculated with M06-2X, an harmonic vibrational analysis (VPT2) was carried out in Gaussian 09.[31] This made only a limited change for most vibrations; the torsion and inversions, which make the largest contributions to the density of states are considered separately.

For all structures, the reaction path was followed to the adduct and to the reactants using the intrinsic reaction coordinate (IRC) method in Gaussian 09.[32] Attempts to optimize a pre-reaction complex on the reagent side of this barrier were made and no stable complex leading to reaction could be found. Single point energies were refined by extrapolating three aug-cc-pVXZ (X=T,Q,5) to the complete basis set limit (CBS) with the CCSD(T) method for M06-2X and CCSD geometries and with QCISD(T) for the QCISD structures using a mixed Gaussian and exponential expression of the form $\mathrm{E(n)} = \mathrm{Ecbs} + \mathrm{Ae}^{-(n-1)} + \mathrm{Be}^{-(n-1)^2}$.[33-35] The scaled zero-point energy corrected values from these treatments will be referred to as CCSD(T)/CBS//M06-2X/ATZ, CCSD(T)/CBS//CCSD/ATZ and QCISD(T)/CBS//QCISD/ATZ, and these are shown in Figure 2 and given in Table 2 (further details on the calculations can be found in the SI, Table S2). Zero-point energy scaling was carried out using the recommended scaling factors taken from CCCBD.[30] The transition-state and C_2H_5 zero-point energies are ~13 and 146 kJ mol^{-1}, respectively.

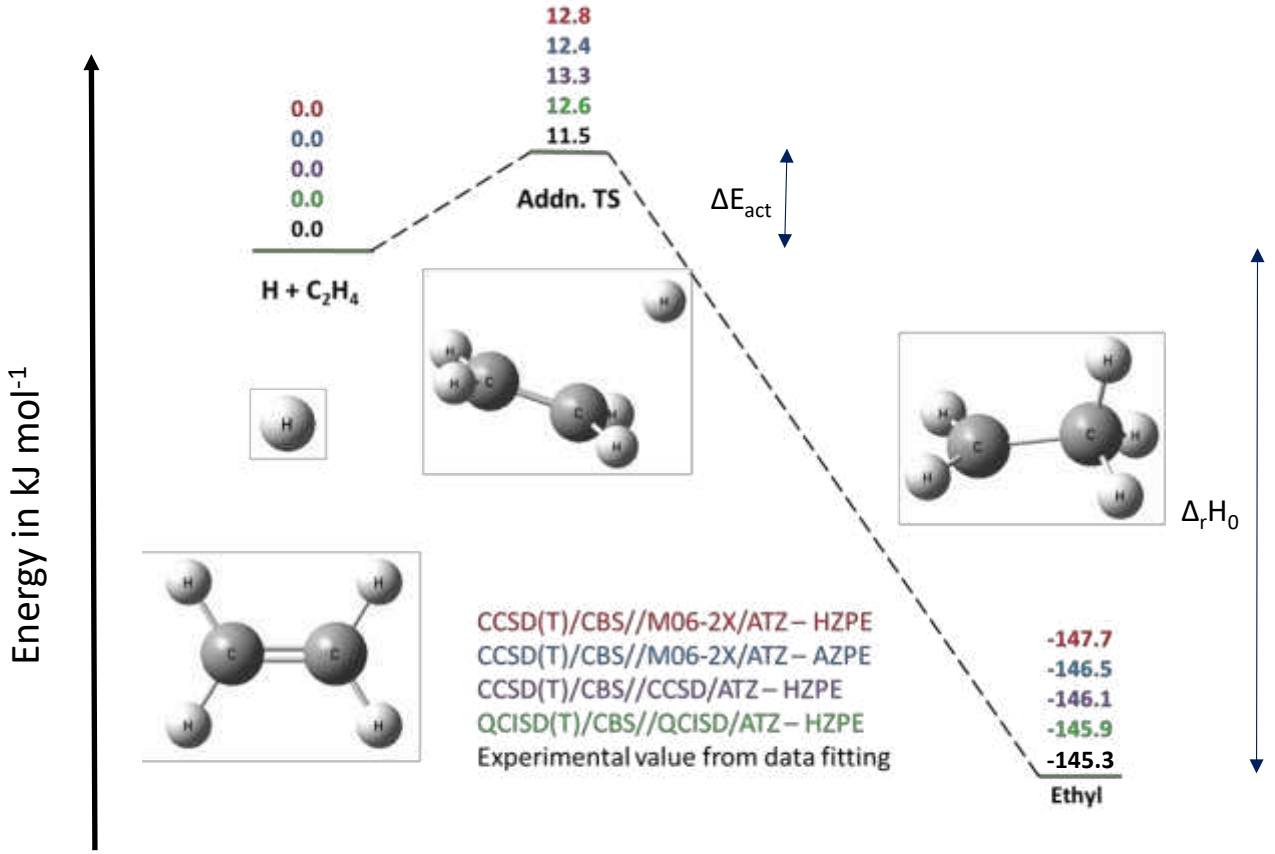

Figure 2. The stationary points in kJ mol^{-1} on the potential energy surface for Reaction 1 and schematics of the molecular configurations. As can be seen, the reaction has a significant barrier and therefore tunneling must be considered.

Table 2. Results of the *ab initio* calculations at various levels of theory.

Method	ΔE_{thresh} H + $C_2H_4 \rightarrow C_2H_5$ / kJ mol^{-1}	$\Delta_r H_0^{\ominus}$ /kJ mol^{-1}
CCSD(T)/CBS//M06-2X/ATZ	12.4	-146.5
CCSD(T)/CBS//CCSD/ATZ	13.3	-146.1
QCISD(T)/CBS//QCISD/ATZ	12.6	-145.9
QCISD(T)/∞//QCISD(*T*)/cc-pvtz [28]	11.8	-146.4
Previous studies	11.7 [36], 12.8 [37], 11.3 [38], 10.5 [39]	-145.3 [37]

The results from the *ab initio* calculations provided the main input parameters for the MESMER description of reaction, R1. The calculated harmonic vibrational frequencies, when corrected for small amplitude vibrational anharmonicities (see Table S3), closely match the experimental frequencies of the species of the system and were used.. The two lowest vibrational frequencies of ethyl are not experimentally well defined and correspond to modes that are not well described by harmonic motion, even if the frequencies are corrected for higher order terms in the PES expansion about the equilibrium. These motions are the torsional motion about the central C-C bond, and the inversion, or wagging, motion of the H atoms of the CH_2 group. To better describe these motions relaxed dihedral scans were carried out. Fully relaxed scans showed that these two motions are coupled to each other, and this coupled 2D surface was mapped out in MOLPRO 2012. [40] As will be discussed shortly, MESMER is only capable of accepting 1D dihedral scans, so relaxed scans were carried out individually for the torsion and the inversion using Gaussian 09. Of these two motions, the hindered rotor is the more important mode in accurately determining the enthalpy of reaction.

3.2 Density of States, $\Omega(E)$

For some time now, there has been an increased focus on calculating $\Omega(E)$ accurately[20].[41] This has been prompted by the realization that while *ab initio* electronic methods have advanced considerably, in many cases to the point of achieving chemical accuracy, the motion of the nuclei has received comparatively less attention. So, it is often the crudeness of the methods used to calculate rovibronic $\Omega(E)$ that contributes most to the overall calculation error. For example, the rigid rotor harmonic oscillator (RRHO) model is still often applied to systems which are neither rigid nor whose vibrations are entirely harmonic, and often leads to $\Omega(E)$ having the wrong energy dependence.

Improvements to the RRHO model have been proposed by a number of workers: Barker and co-workers have tackled the problem of coupled oscillators, a feature that cannot be addressed using direct count methods, by using a restricted Monte-Carlo integration approach of the phase volumes[42] and have applied this to a number of systems (see Barker et al.[43] for a recent example).

Another type of mode that has been singled out for special attention from early on is that of internal rotation. Internal rotors are typically hindered and can impact the calculation of $\Omega(E)$ in three ways: firstly, they are strongly anharmonic, and this leads to a significantly different energy dependence compared to the harmonic oscillator. Secondly, their large amplitude nature means that Coriolis coupling between internal and external rotation can be significant. Thirdly, for long chain molecules (e.g. alkanes longer than propane) the internal rotations can cause changes to the moments of inertia of the molecule, a further mode of coupling. Early work, by Pitzer and Gwinn[44] on the canonical partition functions, $\mathrm{Q}(\beta)$ (the Laplace transform of $\Omega(E)$), of semi-rigid molecules (e.g. methylated benzene compounds) addressed Coriolis interactions at the classical level. Gang et al.[45] reported a full classical solution for all three issues in terms of a phase space integral for $\mathrm{Q}(\beta)$ which was evaluated using Monte-Carlo integration of the corresponding configuration integral against the MM2[46] and MM3[47] potentials, which allowed for non-local potential effects (e.g. end-to-end interactions) to be accounted for. The $\Omega(E)$ can be obtained by inverse Laplace transform (ILT) and this has been implemented in MESMER. Trying to deal with these three issues quantum mechanically is difficult, and it is often the case that the hindered rotor systems are decoupled and solved as 1D Schrodinger equation, obviously excluding some, or nearly all, of the effects described above. Truhlar and co-workers[48-49] have proposed an alternative approach to evaluating $\mathrm{Q}(\beta)$, Multi-Structural Torsion, which takes an average over configurational minima and uses correction factors for anharmonicities. This approach does not appear to account for Coriolis effects, and only partially solves the problem of moment of inertia changes and anharmonicities, and is it is not clear how $\Omega(E)$ would be obtained but does account for quantum mechanical effects. Another quantum mechanical approach is the path integral method as deployed by Clary and co-workers.[50-52] This approach does rigorously deal with all potential anharmonicities but because only the decoupled kinetic energy operator is used will not account for Coriolis or other kinetic couplings between internal rotors.

Of the three species involved in the title reaction it is the ethyl radical that presents most difficulties when considering $\Omega(E)$. The other two species are, by comparison, relatively straightforward: the H-atom is assumed to be in its ground state and thus has a spin degeneracy of 2, while the ethene molecule is well approximated as a closed shell RRHO system and its $\Omega(E)$ can be calculated as a convolution of vibrational states determined by the Beyer-Swinehart[53] algorithm with the rotational states obtained from the full quantum mechanical solution for an asymmetric top. The only other modification made to the ethene $\Omega(E)$ is that a rotational symmetry correction of 4 is applied to account for the fact that the symmetry of ethene molecule belongs to the D_{2h} point group.

As already stated, the ethyl radical exhibits large amplitude motions, specifically a hindered rotor and inversion mode, and so cannot be accurately represented as a RRHO system. As Kreglewski and Gulaczyk[54] demonstrated, the potential of the hindered rotor and the inversion are coupled, so strictly speaking these terms should be treated together, as these authors did. (This behaviour is typical of inversion, see also Ruscic and co-workers[55]). Figure S1 in the SI shows a plot of the internal rotation-inversion potential, which resembles that obtained by Kreglewski and Gulaczyk. The barrier height calculated is 20 cm^{-1} in excellent agreement with the 22 cm^{-1} calculated by Kreglewski and Gulaczyk. The key feature of this plot is that the potential repeats along the torsion-axis every $2\pi/3$ radians hence a symmetry number of 3 is applied to the calculation of the ethyl $\Omega(E)$ to account for this symmetry. Also, there is a symmetry factor associated with inversion because rotation about

the saddle point by π radians would leave the surface unchanged, thus leading to an additional symmetry number of 2. Hence a total symmetry factor of 6 was applied.

Kreglewski and Gulaczyk presented a full solution of the Schrodinger equation for the coupled rotation, inversion and hindered rotor degrees of freedom, and where thus able to converge states up to 600 cm^{-1} or about 7.2 kJ/mol. As figure 2 indicates, the threshold for the dissociation of the ethyl radical is considerably in excess of this value, making a full state specific solution difficult and so a more pragmatic approach to the density of states was taken, based on the assumptions that is phase space volumes rather than exact state values that are the principal determinant. Of the interaction terms discussed above, the alteration of the moment of inertia of the ethyl radical because of internal rotation can be neglected, as these do not change significantly because of the symmetry of the methyl group, and, while the inversion can cause larger changes, these too can be neglected in comparison to other terms. Equally, Coriolis terms will be assumed to be weak for the ethyl radical as motion mostly concerns that of H-atoms causing only a small perturbation of energy levels that is unlikely to substantially alter $\Omega(E)$. Hence the external rotation can be treated as approximately rigid and decoupled from the other modes, and the associated states calculated as the full quantum mechanical asymmetric rotor solution. The remaining modes are all treated as decoupled harmonic oscillators with the exception of the internal rotation and inversion modes. These latter modes were assumed to be approximately decoupled from each other and the other modes and treated using one-dimensional approximations.

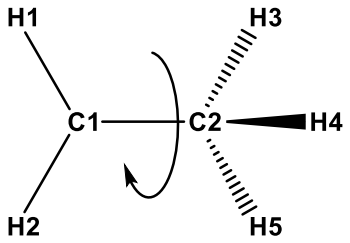

Scan of the dihedral angle represented by
H1-C1-C2-H3
gives the torsional potential

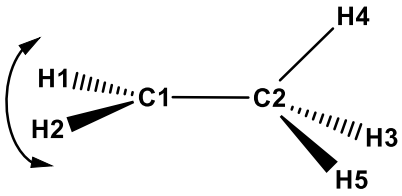

Scan of the dihedral angle represented by
C1-H1-H2-C2
gives the inversion potential

Figure 3. Schematic figures showing the angles scanned to generate the potentials.

For the internal rotation, the effective potential of 20 cm^{-1} was found through a relaxed dihedral scan, which optimized each point around the central C-C bond, see Figure 3 above and Figure S1. The hindered rotor states were calculated by forming a Fourier expansion of the potential and using these terms in a Hamiltonian representation based on one-dimensional free rotor eigenfunctions (see Glowacki et al.[12] for details). The inversion potential was obtained by identifying its dihedral angles and then carrying out a relaxed dihedral scan which was optimized at each point. This dihedral angle is that between the plane of the carbon and hydrogen atoms of the CH_2 group, see Figure 3. These relaxed dihedral scans were carried out at the M06-2X/aug-cc-pVTZ level in Gaussian 09.[29] Once the inversion potential was obtained, the eigenstates were calculated by applying the

Fourier Grid Hamiltonian method of Stare and Balint-Kurti.[56] Finally, these eigenstates were convolved with the internal and external rotational eigenstates and the regular harmonic oscillator eigenstates used to represent all other vibrational modes to give the overall $\Omega(E)$.

Having obtained the densities of states for all species participating in the reaction, the next step is to consider the determination of the sum of states at the transition state, $\mathrm{W}(E)$, which is needed to estimate of microcanonical rate coefficients via microcanonical transition state theory. In their analysis, Miller and Klippenstein[28] noted that the barrier to association is low and consequently employed flexible transition state theory (FTST), a variational treatment that accounts for the effects of angular momentum coupling and other kinematic effects. Typically, FTST is applied to barrierless reactions, such as the recombination reaction of methyl radicals to give ethane and broadly speaking it is observed that the transition state location along the minimum energy path (MEP) tends to large separations for small association energies (or conversely dissociation energies that are just above the threshold) and that it moves to smaller separations as the energy is increased. In the present case, the presence of a barrier to association means that for low energies the flux minimum will almost certainly be in the vicinity of the maximum of the barrier. From the point of view of dissociation, the minimum in the flux will again be close to the transition state. So, it was assumed in the present analysis that the transition state is always located at the top of the barrier. However, given that the reaction involves a hydrogen atom, and so quantum mechanical tunneling is likely to be significant, the Eckart tunneling approach used by Miller[57] and commonly used in other studies, was also employed in the model.

4. Global Fitting: Fitting Criteria and Experimental Dataset

When describing a reaction using a ME, there is often a significant degree of uncertainty in a number of its parameters. MESMER has the facility to adjust several of the parameters that strongly influence the kinetics of the reaction to best fit the model to experimental data, and hence define the adjusted parameter, together with its uncertainty. In our previous study on peroxy radicals association with NO_2, MESMER fitting highlighted that the adduct binding energy was defined to better than 1 kJ mol^{-1} [15] and in the more recent study on the OH addition with C_2H_4[16] a defined binding energy was obtained that was in excellent agreement with a high level *ab initio* calculation.[58]

Experimentally, as well as the kinetic data on H + C_2H_4 given in Table 1, there is a considerable number of previous studies which are summarized in Table 3. These data have been combined with the measurements reported herein and fitted to determine specified parameters of the system. The parameters of the system investigated are (see also Fig. 2): the enthalpy of reaction at 0 K ($\Delta_r H_0^{\ominus}$), the transition-state threshold to reaction with ZPE correction (ΔE_{thresh}) and the imaginary frequency of the transition-state (υ_{imag}). The imaginary frequency is used to describe the quantum mechanical tunnelling via an Eckart model.[57] In addition, the energy transfer parameters for each buffer gas are required in the MESMER data fitting as the reaction is not at its high-pressure limit. MESMER uses the exponential down model for energy transfer where $\langle \Delta E \rangle_d$ is the average energy transferred in a downward direction and is given by:

$$\langle \Delta E \rangle_d = \langle \Delta E \rangle_{d,298} (T/298)^n \quad (1)$$

where $\langle \Delta E \rangle_{d,298}$ and *n* can be varied for each bath gas in the MESMER fitting routine.

The MESMER model parameters were fitted by optimizing the figure of merit function χ^2:

$$\chi^2 = \sum_{1}^{N} (k_{i,expt} - k_{i,model})^2 / \sigma_i^2 \quad (2)$$

where $k_{i,expt}$ and $k_{i,model}$ are the experimental and modelled rate coefficients, respectively, for each individual pressure and temperature, *i*, over all experiments, *N*, and σ_i is the standard deviation for each experimental point.

Perhaps the main difficulty encountered in this work is that not all studies reported errors. In certain circumstances an "average" error can be derived,[59] the basis of which is the observation that, for a moderately good fit,[59-60] χ^2/N_{dof} (where $N_{dof} = N - N_p$ is the number of degrees of freedom, N_p being the number of parameters being fit) should be close to unity. However, this requires data to be on the same scale which in the present case they are not, as dissociation and association data are being combined and these data are on different scales. For the present study, a pragmatic modification of this approach was adopted. The wide range in scales suggest that errors should be assigned as a ratio of the data values, that is as x% of the data values, and we have taken x = 10 as a reasonable estimate. If it is assumed that the errors are approximately independent then, again, it is expected that χ^2/N_{dof} should be close to unity. For the results presented below x was typically in the range 10-20.

As with the simple "average" error model, deriving the errors in this way precludes any assessment of the veracity of the underlying model, as a moderately good fit is assumed. It also does not make any provision for systematic errors, but it does allow data from different sources to be combined. This approach was implemented using MESMER where the optimal value of χ^2 was obtained using the Levenberg-Marquardt algorithm.[59]

As indicated above the determination of the parameter values used data from a number of sources in addition to the present measurements. Combining data from different sources is difficult because a given data set is almost certainly delivered, to some extent, with a systematic bias, either from the experimental method or the subsequent analysis of the data. Thus, deciding which data sets are to be combined, how they are to be weighted and which parameters they are going to be used to fit requires care. Table 3 lists all the data sets that were used in the present analysis.

Table 3. Data sets used in the analysis of the title reaction.

Label	Study	Bath Gas	Temperature Range /K	10^{-17} [M] /molecule cm^{-3}	Rate Coefficients Measured [a]	Technique [b]
A	Lightfoot and Pilling [61]	He	284-604	9.5 - 140	A	LFP/RF
B	Present work	He	796-828	23 – 72	A/D	LFP/LIF
C	Hanning-Lee et al. [11]	He	800	12 – 72	A/D	LFP/RF
D	Brouard et al. [10]	He	775-825	25	A/D	LFP/RF
E	Kurylo et al. [62]	He	300	2.3 – 160	A	FP/RF
F	Michael et al. [63]	He	300	0.17 – 190	A	HgP/F/RA
G	Barker and Michael [64]	He	300	0.087 – 1.6	A	DF/RA
H	Barker et al. [65]	He	300	0.26 – 1.6	A	DF/RA, HgP/P/RA, DF/TOF
I	Feng et al. [17]	He	876-1094	0.071 – 1.6	D	LFP/PIMS
J	Lin and Back. [66]	C_2H_6	823-913	3.8 - 69	D	Pyr/GC
K	Loucks and Laidler [67]	C_2H_6	670-773	0.43 – 87	D	HgP/GC
L	Pacey and Wimalasena [68]	C_2H_6	902	1.1 – 27	D	Pyr/GC
M	Trenwith [69]	C_2H_6	841-913	1.1 – 100	D	Pyr/GC
N	Simon et al. [70]	C_2H_6	793-813	0.12 – 37	D	Pyr/GC
O	Lee et al. [71]	Ar	198 - 320	130 – 180	A	FP/RF
P	Michael et al. [63]	Ar	300	0.31 – 4.7	A	HgP/F/RA
Q	Sugawara et al. [72]	H_2	456	23 – 290	A	PR/RA
R	Sugawara et al. [72]	H_2	211-461	Not specified	A	PR/RA
S	Michael et al. [63]	H_2	300	0.33 – 8.0	A	HgP/F/RA

a – A = Association only, D = Dissociation only, A/D Approach to equilibrium yielding both association and dissociation rate coefficients.

b - Techniques: LFP: laser flash photolysis; FP: flash photolysis; RF: resonance fluorescence; RA: resonance absorption; LIF: laser induced fluorescence; DF: discharge flow; HgP: mercury photosensitized dissociation (F: in flow system; P: pulsed); TOF: time of flight mass spectrometry; PIMS: photoionization mass spectrometry; Pyr: Pyrolysis; GC: gas chromatography; PR: pulse radiolysis.

Ideally the number of parameters in a fitting exercise should be kept to a minimum, because an over- parameterized fitting function can have considerable flexibility and as a consequence can lead to overfitting giving a misleading assessment of parameters values. As stated above, the target parameters include PES features and energy transfer parameters. PES parameters are most sensitive to temperature while energy transfer parameter information is best obtained from data at different bath gas concentrations. With these general notions in mind a strategy was developed to assess the data as follows:

- Data sets using a single bath gas should be used to determine the PES parameters, in order to limit the number of variable parameters.
- The bath gas data sets to be used to fit the PES parameters should be those with the greatest temperature range, preferably with good low temperature coverage, given the importance of tunnelling.
- Once the PES parameters have been determined from the identified combination of data sets, these parameters, along with the energy transfer parameters of the selected bath gas, should be fixed.
- Analysis of the other data sets, which refer to different bath gases should use these fixed PES parameters to infer the energy transfer parameters of the other bath gases.

Once this process was complete, a final check was performed using all those datasets consistent with the PES fitting parameters the expectation being that the parameter set should not change significantly. Small changes were observed but only in the fifth or sixth significant figure for the key PES parameters. There are weaknesses in this strategy, the main one being that bias in the determined PES parameters can affect subsequent determination of energy transfer parameters. However, in the absence of any information about such a bias, these parameters constitute the best available estimates.

Inspection of Table 3 indicates that data with helium as the bath gas traverses the low and high-temperature regimes, where time-resolved measurements have determined both k_1 and k_{-1}. Therefore, the helium data sets A - I [10-11, 17, 61-65] were used as the starting point for the analysis. The high temperature data are dominated by several studies where ethane is the buffer gases.[66-70] These ethane datasets were assessed by fixing PES parameters obtained from fitting the He data set combination, the object being to extract energy transfer parameters. Similarly, energy transfer parameters for other bath gases were obtained by first fixing the PES parameters.

5. Data Fitting: Results and Discussion

As discussed above in section 4, how data sets are combined, and parameter values extracted needs care. As also discussed, limiting the number of parameters fitted at any one time is important and as a consequence the strategy outlined above was adopted whereby the data for which He is the bath gas should be used to infer PES parameters.

Table 4. Summary of parameters from fits to $C_2H_4 + H \rightleftarrows C_2H_5$ with He as the buffer gas. Errors are 2σ.

Model and Comments	χ^2	χ^2/ degree of freedom	*N*	$\Delta_r H_0^{\ominus}$/kJ mol^{-1}	$\langle \Delta E \rangle_{d,298}$ (He)/ cm^{-1}	*(T*/298*)*^{n}$_{He}$	υ_{imag}/cm^{-1}	ΔE_{thresh} / kJ mol^{-1}	
Fully optimized hindered rotor (HR) torsion and inversion as discussed above	149	1.39	112	-145.34 ± 0.60	54.2 ± 7.6	1.17 ± 0.12	730 ± 130	11.43 ± 0.34	
Miller and Klippenstein [28] *ab initio* calculation				-146.36	75	0.95	765	11.76	
HR torsion only, see Fig 3.	145	1.35	112	-145.22 ± 0.60	48.5 ± 6.6	1.22 ± 0.12	780 ± 130	11.54 ± 0.36	
HR torsion and inversion calculated while torsional mode frozen.	144	1.35	112	-144.73 ± 0.58	48.3 ± 6.6	1.23 ± 0.12	790 ± 130	11.55 ± 0.36	
Vib1 using experimental value for HR torsion 20 cm^{-1}, [73]	182	1.69	112	-138.37 ± 0.54	30.2 ± 4.0	1.24 ± 0.12	850 ± 130	12.07 ± 0.40	
Vib2 using calculated value for HR torsion 122 cm^{1}	149	1.39	112	-149.98 ± 0.60	51.1 ± 7.0	1.17 ± 0.12	740 ± 130	11.45 ± 0.34	
Model and Comments	χ^2	χ^2/ degree of freedom	*N*	$\Delta_r H_0^{\ominus}$/kJ mol^{-1}	$\langle \Delta E \rangle_{d,298}$ (He)/cm^{-1}	*(T*/298*)*^{n}$_{He}$	A/10^{-11} cm^3 molec^{-1}s^{-1}	E_{act}/ kJ mol^{-1}	*n*
ILT	152	1.42	112	-145.32 ± 0.60	67.3 ± 12.8	1.00 ± 0.16	2.20±1.88	7.7 ± 2.2	0.98 ± 0.75

5.1 Fits to Different Bath Gases

5.1.1 Helium

An initial fit was performed with data sets A to I inclusive. The optimal values for the floated parameters are given in the top row of Table 4. The values obtained are consistent with the *ab initio* calculations described above and also with the high-level *ab initio* calculations performed by Miller and Klippenstein [28] who reported $\Delta_r H_0^{\ominus} = -146.36\ \mathrm{kJ\ mol^{-1}}$, $\Delta E_{thresh} = 11.76\ \mathrm{kJ\ mol^{-1}}$, and υ_{imag} = 765 cm^{-1}. Miller and Klippenstein also reported $\langle \Delta E \rangle_d = 75(T/300K)^{0.95}$ cm^{-1} which differs from the values observed here but does, none-the-less, support a near linear temperature dependence of $\langle \Delta E \rangle_d$. The correlation coefficient matrix for the fit is given in Table 5. The correlation coefficient matrix shows there is a significant correlation between ΔE_{thresh} and υ_{imag} which is to be expected, since υ_{imag} is related to the width of the barrier (the larger the value the narrower the barrier) and ΔE_{thresh} is related to the height of the barrier. The positive correlation is consistent with an increasing barrier height being counteracted by an increase in tunnelling by narrowing of the barrier to obtain the same rate coefficient. There is also a strong negative correlation between $\langle \Delta E \rangle_{d,298}$ and n which is also to be expected. The origin of the correlation between υ_{imag} and $\langle \Delta E \rangle_{d,298}$ and υ_{imag} and n is less clear. Finally, the $\Delta_r H_0^{\ominus}$ parameter appears to be only weakly correlated to the other parameters suggesting that this parameter is well defined.

Table 5. Correlation Coefficient matrix for the He bath gas fit.

	$\Delta_r H_0^{\ominus}$	ΔE_{thresh}	υ_{imag}	$\langle \Delta E \rangle_{d,298}$	n
$\Delta_r H_0^{\ominus}$	1.0				
ΔE_{thresh}	-0.124	1.0			
υ_{imag}	-0.121	0.818	1.0		
$\langle \Delta E \rangle_{d,298}$	0.207	-0.283	-0.749	1.0	
n	-0.380	0.346	0.755	-0.971	1.0

Figure 4 shows the reduced residuals (($k_{expt} - k_{fit}$)/ k_{expt}) from the best fit, with each of the experimental studies labelled. The x-axis is the number of the result, in the order shown in Table 3, i.e. results 1 - 18 are those from set A by Lightfoot and Pilling[61] at 284 - 604 K, which includes 18 rate coefficient measurements at pressures in the range 50 – 700 Torr. For datasets A – H, the data have been grouped initially as a function of temperature and then within each temperature range as a function of pressure. For dataset I (Feng et al.[17]) very few measurements are made at the same temperature and so the data are binned into increments of ~10 K and then arranged in order of increasing [M] in each temperature bin. The data used are presented in the SI (Table S4). The figure shows the results of fits for both association and dissociation rate coefficients. All are based on direct measurements using discharge flow or pulsed photolysis with detection using resonance absorption, resonance / laser induced fluorescence or mass spectrometry. Altogether there are 112 measurements. The data are randomly scattered, although individual measurement sets show some bias against the best fit values. The dissociation measurements of Feng et al. show the least scatter, but they do show a systematic decrease in the value of the residual with experiment number, i.e. with increasing temperature, and within each temperature bin, there is generally a systematic

increase with pressure, suggesting either an experimental artefact or a deficiency in the energy transfer model. We return to this issue in section 5.3.3.

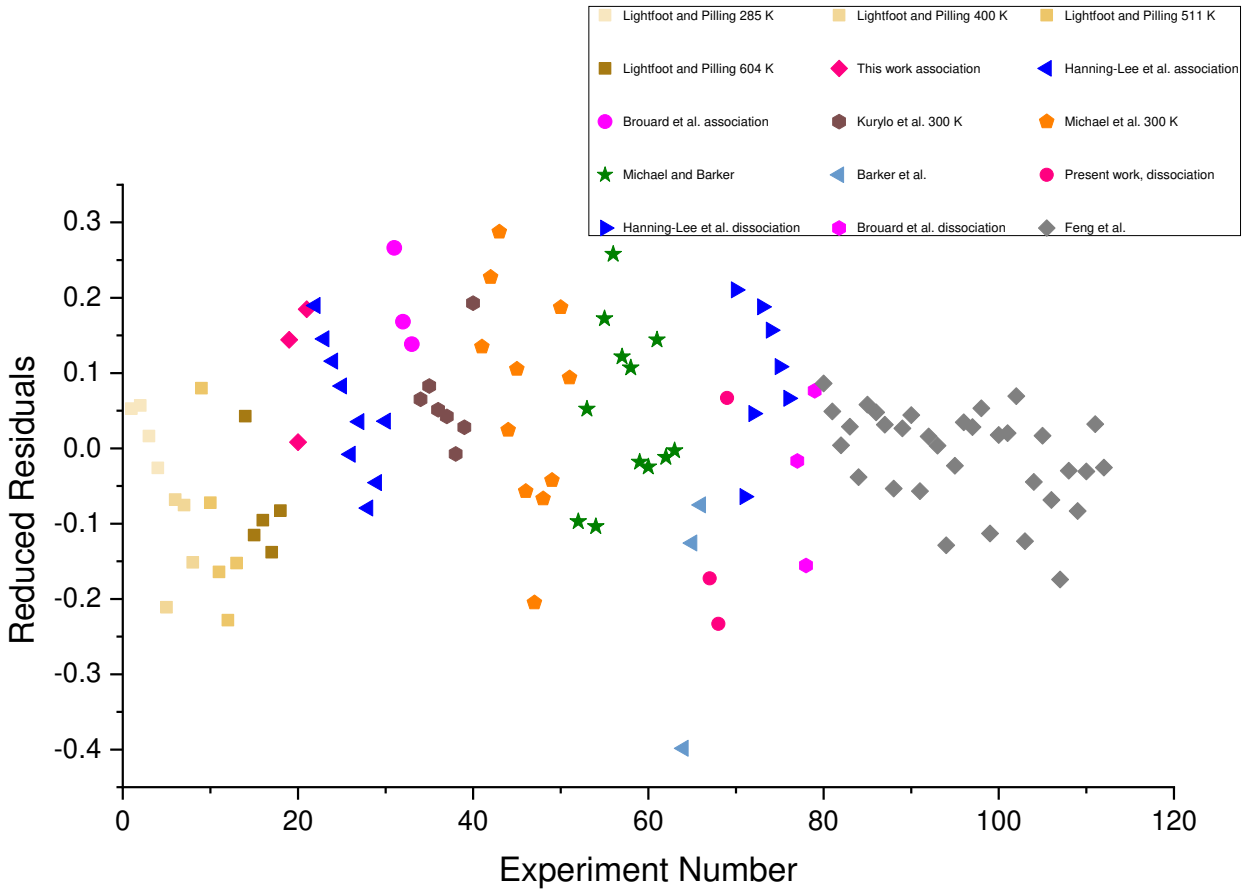

Figure 4. Reduced Residuals $\left(\frac{k_{expt}-k_{fit}}{k_{expt}}\right)$ for the various experiments where helium is the bath gas. The full set of conditions for each experiment can be found in Table S4 in the SI.

This combination of data sets was also used to assess, in a limited way, the quality of the density of states calculation for the ethyl radical and the impact of using less accurate models. Table 4 shows the results of fitting the He data with other models. Two harmonic vibration-only models were examined. In one, Vib1, the experimental frequency obtained by Sears et al.[73] of 20 cm^{-1} was used for the internal rotor; in the other, Vib2, the *ab initio* value of 122 cm^{-1} was used. A frequency of 477 cm^{-1} was used for the inversion. These vibration models give parameters that differ considerably from the hindered rotor model result given above, with the low frequency model (Vib 1) giving a low, and the high frequency model based on the *ab initio* value (Vib 2) giving a high value for the enthalpy of reaction. These results demonstrate the importance of a realistic description of the internal rotor in calculating the densities and sums of state for ethyl.

The other mode discussed above is the inversion at the radical centre, which the potential energy surface diagram in Figure S1 shows is anharmonic. The impact of this mode was tested in two ways:

- The torsion potential for the internal rotor mode was retained, but the inversion mode was replaced by a harmonic oscillator, 504 cm^{-1}.
- The torsion potential for the internal rotor was retained, but the inversion potential was that obtained with a fixed geometry for the rest of the molecules; this model is less realistic.

These give results that lie within the uncertainty range of the main fit to the data, although $\langle \Delta E \rangle_{d,298}$(He) is slightly reduced and υ_{imag} slightly increased, suggesting that inversion effects are limited for the ethyl radical.

Miller and Klippenstein[28] used a variational 2D model in the theoretical analysis of the title reaction. The MESMER fitting process was only able to accommodate a fixed transition state model. As discussed below in section 5.3.1, this leads to a $k_1^{\infty}(T)$ expression that slightly exceeds that of Miller and Klippenstein at high temperatures. In order to check whether this led to errors in the enthalpy change of reaction, microcanonical rate constants for ethyl dissociation were determined by inverse Laplace transformation (ILT) of the high-pressure limit for association, expressed in the form $AT^n \exp(-E_{act}/RT)$, where A , n and E_{act} are fitting parameters. This approach is often used, especially for association reactions with no barrier.[74] The results are shown in the last row of Table 4. The best fit enthalpy change of reaction is unaffected, although $\langle \Delta E \rangle_d$ for He is somewhat increased. The E_{act} parameter obtained is smaller than the barrier threshold. Since the microcanonical rate constants for the ILT model are strictly zero below the threshold, we speculate that the fitting process has generated this low energy to accommodate some of the effects of tunnelling.

5.1.2 Ethane

The dissociation experiments with ethane (data sets J-N) all used end-product analysis. Data sets J, L, M and N were based on ethane pyrolysis and data set K used mercury photosensitized dissociation of ethane. Studies J, K, M and N used static systems whereas Pacey and Wimalasena (data set L) used a flow reactor. The temperatures were in the range ~700 – 1000 K, with pressures of ethane of ~ 1-900 Torr. The temperature range for each set of measurements was ≤ 100 K.

Following the strategy outlined above, the analysis of these data began by fixing the PES parameters at the values obtained from fitting the He based data. A fitting exercise was then run which includes data from all sets J-N, with the energy transfer parameters $\langle \Delta E \rangle_{d,298,\mathrm{C2H6}}$ and n of Eq. (1) floated. This gave a poor fit with substantial scatter and parameter values of: $\langle \Delta E \rangle_{d,298} = 684 \pm 66\ \mathrm{cm}^{-1}$ and $n = -0.791 \pm 0.094$ (errors are 2 standard deviations). Both the substantial scatter and the unrealistic parameters (both the size of $\langle \Delta E \rangle_{d,298,\mathrm{C2H6}}$ and, in particular, the sign of n, which contradicts the generally accepted notion that energy transfer in a collision increases with temperature) indicated a poor fit. Inspection of the data on an experiment vs calculated scatter plot revealed that set M showed considerable scatter compared to the other sets and occupied a different region of the plot. While this measure is somewhat subjective, it was decided to remove set M from the data to be fit and execute a further fit. The results from this fit (excluding data set M) were: $\langle \Delta E \rangle_{d,298,\mathrm{C2H6}} = 91 \pm 10\ \mathrm{cm}^{-1}$ and $n = 1.48 \pm 0.11$ (note that $\langle \Delta E \rangle_{d,298,\mathrm{C2H6}}$ will be ~400 cm^{-1} at 800 K, approximately the midpoint temperature of the ethane experiments) The temperature dependence of this model is somewhat stronger than the case of He, which might be

a consequence of greater vibrational activation at higher temperatures; this result is consistent, though, with the general energy transfer characteristics for gas phase systems.[75-76] However, Figure 5a shows that whilst the above reasonable values for the energy transfer parameters can be obtained, the data of Simon et al.[70] and Loucks and Laidler[67] appear to have some systematic errors with non-random distributions of the residuals. (Again, the data have been grouped into temperature ranges (see SI, Table S5)). A final analysis just using the data of Lin and Back[66] and Pacey and Wimalasena[68] gives an acceptable fit (see Figure 5b) with χ^2/N_{dof} = 0.97 with $\langle \Delta E \rangle_{d,298} = 510 \pm 160\ \mathrm{cm}^{-1}$ and $n = 0.00 \pm 0.29$. For an atomic species, where impulsive collisions dominate, a positive temperature dependence is expected for the energy transfer parameter. For ethane, there will still be this positive temperature dependent component of energy transfer, but this can be offset by V-V mechanisms which generally have a negative temperature dependence, i.e. they are facilitated by complex formation. Therefore, our value, close to temperature independent, appears reasonable. However, there is a significant uncertainty in the temperature dependence that is not surprising considering the smaller range of temperature covered by Lin and Back and Pacey and Wimalasena, compared to the full ethane dataset. More extensive consistent data are required to fully constrain the energy transfer parameters for ethane.

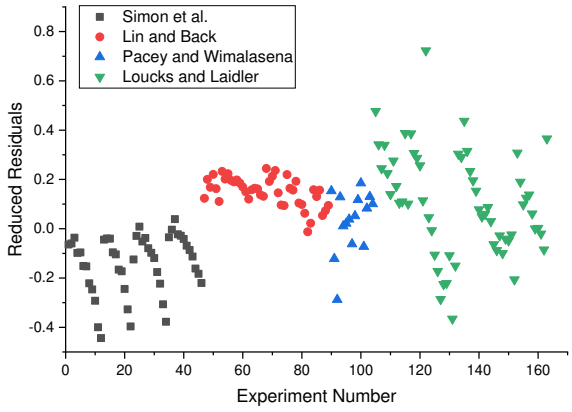

Figure 5a. Reduced residuals plot showing the systematic variations in data of Simon et al. and Loucks and Laidler, even after the values of Trenwith have been removed.

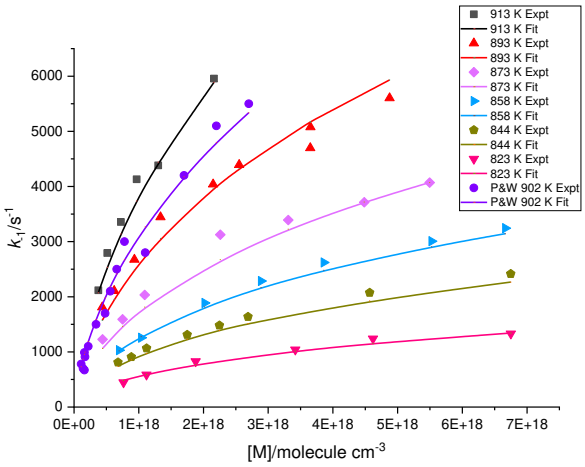

Figure 5b. MESMER fits to the experimental data of Lin and Back with PES parameters constrained to the values from the He data with $\langle \Delta E \rangle_{d,298} = 510 \pm 160\ \mathrm{cm}^{-1}$ and $n = 0.00 \pm 0.29$.

An alternative approach to considering the consistency of the ethane datasets by examining the effects of adding each ethane bath gas dataset to the base helium bath gas dataset is shown in the SI (Section 7). Table S6 shows the variation in both χ^2/N_{dof} and the PES parameters for each data set. A similar conclusion is reached to the above analysis.

The datasets of Trenwith, Simon et al. and Loucks and Laidler have been excluded based on the quality of the fits. Examination of these papers shows that all of these studies were carried out in relatively small reactors (< 1 dm^3), hence with a high surface to volume (S/V) ratio and potential for

heterogeneous processes and that no checks were made for variations in S/V ratios. In contrast, Pacey and Wimalasena used a flow system and carried out their experiments in different reactors with a range of S/V ratios. Lin and Back did use a static system, but investigated S/V effects and measured a wider range of end products. Additionally the values of the ethyl dissociation rate coefficient were typically a factor of ten higher than many of the other studies, so that the effects of secondary chemistry are likely to be less significant. Lin and Laidler[77] jointly analysed their respective data using RRK analysis. They were systematically unable to fit the lower pressure Hg photosensitization data of Loucks and Laidler and suggested that the low pressure data were influenced by dissociation of chemically activated ethyl radicals.

5.1.3 Other third bodies

Michael and co-workers[63] measured k_1 in the bath gases Ar, H_2, Ne, Kr and N_2 at 300 K and at pressures in the range ~ 1 – 25 Torr, using a flow technique, coupled with resonance absorption. H was generated by Hg photosensitized dissociation of H_2. In the present work, these data were fitted using the PES data from the He fits to obtain values for $\langle \Delta E \rangle_d$ for each bath gas giving 65.0 ± 4.5 cm^{-1} (Ar), 30.0 ± 2.3 cm^{-1} (H_2), 70.5 ± 6.4 cm^{-1} (Ne), 76.0 ± 7.3 cm^{-1} (Kr) and 62.2 ± 5.5 cm^{-1} (N_2) Errors are 2 standard deviations. They also made measurements with SF_6 as the bath gas, but it was not possible to fit these data with realistic energy transfer parameters.

Lee et al.[71] used flash photolysis/ resonance fluorescence to measure k_1 over the temperature range 198 - 320 K and at Ar pressures of ~300 – 760 Torr. Only one or two pressures were employed at each of seven temperatures. Sugawara et al.[72] employed pulse radiolysis of H_2/C_2H_4 mixtures, coupled with resonance absorption, at temperatures of 211 – 461 K. H_2 was in great excess and acted as the third body. At 456 K they measured k_1 at pressures from ~100 – 1400 Torr and showed that the reaction was approaching the high-pressure limit at the higher pressures, although they did not perform an analysis of the pressure dependence. At the other temperatures they operated at a high, unspecified pressure and quoted the resulting rate constants as the high-pressure limits. In our analysis, we assumed that they had used a pressure of 760 Torr.

As for the ethane data, fits for Ar bath gas data sets, O and P, and H_2 bath gas data sets, Q and R, were performed keeping the PES parameters fixed at the values determined in the fitting of the He bath gas data. For Ar an initial fit with just $\langle \Delta E \rangle_d$ floated was performed and this gave a value of $73.8 \pm 8.06\ \mathrm{cm}^{-1}$, which is consistent with the low-pressure measurements of Michael et al. (65.0 ± 4.5 cm^{-1}). The small amount of data in the combined O and P sets means even more caution is needed when contemplating adding extra parameters to a fit, however, two other exploratory fits were conducted. In the first, the full expression given in Eq. (1) was floated. The fit obtained was not significantly better in terms of χ^2. The parameter values obtained were $\langle \Delta E \rangle_{d,298} = 73.9 \pm 9.55\ \mathrm{cm}^{-1}$ and $n = -1.49 \pm 5.12$. The value of n is in contradiction the general notion that energy transfer becomes larger at higher temperature and the errors indicate that there is not enough information in this small set of data close to the high-pressure limit to derive any conclusions about the temperature dependence of energy transfer of Ar to be made. The other exploratory fit that was conducted was to float the height of the activation threshold, ΔE_{thresh}, in order to make some sort of assessment of whether the transfer of PES parameters from the He fit is justifiable. The values

obtained for this fit were $\langle\Delta E\rangle_d = 65.5 \pm 8.2\ \mathrm{cm}^{-1}$ and $\Delta E_{thresh} = 11.17 \pm 0.16\ \mathrm{kJ\ mol}^{-1}$. The fit was significantly better in terms of χ^2 than the preceding two fits. The value of $\langle\Delta E\rangle_d$ from this fit lies within the (2σ) error limits from the preceding two fits, while the value of ΔE_{thresh} lies within the error limits of the He fit. Bearing in mind the small amount of data, this approximate agreement indicates the transfer of PES parameters is acceptable.

A similar analysis was applied to the combined Q, R and S sets where hydrogen is the bath gas. An initial fit with only $\langle\Delta E\rangle_{d,H2}$ floated gave an energy transfer parameter of $48.7 \pm 3.8\ \mathrm{cm}^{-1}$. The quality of the fit was poor with the experimental values from the Q and R data sets being consistently greater than the best-fit values and the experimental values from data set S being consistently lower than the best-fit values. As above, the temperature dependent $\langle\Delta E\rangle_d$ was fitted and in this case a significantly better fit was obtained with $\langle\Delta E\rangle_d = 47.0 \pm 4.2\ \mathrm{cm}^{-1}$ and $n = 1.45 \pm 0.47$, but, again, sets Q and R remained consistently above the fit while data from set S was below. Fits were also done where PES parameters were allowed to float, but for this case there was no significant change in either the PES parameters or the energy transfer parameters all of which remained within the error bars of the fits described so far.

5.1.4 Final Fitting

As a final check on the consistency of results from the various fitting exercises described above, a combined fit for of all sets, excluding sets K, M and N, was done in which the PES and the relevant energy transfer parameters were varied. The expectation for this fit is that there should be only small changes in values because the PES surface parameters are essentially determined by the He data and correlations between energy transfer parameters of different bath gases should be small. The results of this fit are given in the second column of Table 6 along with the parameters from the fit to the helium bath gas experiments.

Table 6. Parameters from a combined fit with He, Ar, H_2 and selected C_2H_6 data compared to those from with only the helium bath gas data.

Parameter	Value from final fit where the errors are 2σ	Values from a fit only to the He bath gas data.
$\Delta_r H_0^{\ominus}$/kJ mol^{-1}	-145.34 ± 0.56	-145.34 ± 0.60
ΔE_{thresh}/ kJ mol^{-1}	11.43 ± 0.30	11.43 ± 0.34
υ_{imag}/cm^{-1}	731 ± 96	730 ± 130
$\langle\Delta E\rangle_{d,298}$(He)/cm^{-1}	54.2 ± 4.5	54.2 ± 7.6
n (He)	$1.175 + 0.079$	$1.17 + 0.12$
$\langle\Delta E\rangle_{d,298}$(Ar)/cm^{-1}	74 ± 10	
n (Ar)	0.001 ± 0.129	
$\langle\Delta E\rangle_{d,298}$($H_2$)/cm^{-1}	46.9 ± 5.6	
n (H_2)	1.41 ± 0.53	
$\langle\Delta E\rangle_{d,298}$($C_2H_6$)/cm^{-1}	$510 \pm 490.$	
n (C_2H_6)	0.001 ± 0.800	

Table 6 shows that the best fit PES parameters remain largely unchanged from the fit to the helium data alone. The values of the energy transfer parameters for Ar and C_2H_6 again reflect the narrow range of temperature at which the experimental data were obtained, coupled with the closeness of the variable temperature data to the high-pressure limit, so that limited information could be extracted of the temperature dependence of the energy transfer of these bath gases.

The correlation coefficients between energy transfer parameters are generally very small as might be expected; the exceptions to this were the correlation coefficients between $\langle\Delta E\rangle_{d,298}$(He) and $\langle\Delta E\rangle_{d,298}$(Ar) which is 0.512 and between $\langle\Delta E\rangle_{d,298}$(He) and $\langle\Delta E\rangle_{d,298}$($H_2$) which is 0.562. This most likely reflects that changes in certain parameters will result in similar changes in all $\langle\Delta E\rangle_{d,298}$, leading to an apparent correlation.

5.2 Parameters for the Potential Energy Surface of Reaction 1

5.2.1 Enthalpies of Reaction and Formation of the Ethyl Radical

The best fit value for the standard enthalpy of reaction at 0 K, $\Delta_r H_0^{\ominus}$ is given in Table 6 as -145.34 ± 0.60 kJ mol^{-1}, where the uncertainty is two standard deviations. This value is primarily determined by the extensive set of data in He. It is relatively insensitive to the model used to determine the microcanonical rate constants (e.g. RRKM or ILT with full treatment of the hindered rotor and inversion) although it was changed substantially if a rigid rotor harmonic oscillator treatment were used (see Table 4). Miller and Klippenstein obtained a value of -146.35 kJ mol^{-1} at their highest level of theory, while the calculations reported here give -145.9 kJ mol^{-1} (QCISD(T),CBS//QCISD/ATZ).

Table 7 gives the enthalpies of formation for H, C_2H_4 and C_2H_5 from the latest version of ATcT. These give $\Delta_r H_0^{\ominus}$ = -145.86 ± 0.30 kJ mol^{-1} in excellent agreement with the value obtained here. Using the enthalpies of formation for H and C_2H_4 in Table 7, together with the enthalpy of reaction obtained in this paper gives $\Delta_f H_0^{\ominus}$(C_2H_5) = 131.55 ± 0.57 kJ mol^{-1}, slightly higher than the ATcT value of 131.04 ± 0.27 kJ mol^{-1} but well within the combined uncertainties.

Table 7. Standard enthalpies of formation from the Active Thermochemical Tables 1.122p.

	$\Delta_f H_0^{\ominus}$	$\Delta_f H_{298.15}^{\ominus}$	Uncertainty (2σ)
H	216.034	217.998	0
C_2H_4	60.87	52.35	±0.12
C_2H_5	131.04	119.98	±0.27

The enthalpy of formation for ethyl at 298.15 K was obtained in two ways. The ATcT value for ($\Delta_f H_{298.15}^{\ominus}$ - $\Delta_f H_0^{\ominus}$) for C_2H_5 is -11.06 kJ mol^{-1}. Combining this with our value for $\Delta_f H_0^{\ominus}$(C_2H_5) gives $\Delta_f H_{298.15}^{\ominus}$ (C_2H_5) = 120.49 ± 0.57 kJ mol^{-1}. Using the molecular parameters obtained from our *ab initio* calculations gives $\Delta_f H_{298.15}^{\ominus}$ (C_2H_5) = 120.64 kJ mol^{-1} in excellent agreement. Both values are slightly higher than that given in Table 7, from ATcT. Tables S7-9 provide the complete thermodynamic data for C_2H_5, C_2H_4 and H, based on the molecular parameters used in the master equation calculations.

It is of interest to examine the impact of the hindered rotor model used in these calculations on H(298.15 K) – H(0 K) for ethyl which is given in Table S7. Fig 6 shows a plot of C_v/R vs T for this mode; a maximum value of 0.77 occurs at 8 K, but the classical value of 0.5 is established, within 1%, by 23 K. The impact of the low temperature non-classical behaviour shown in Fig 6 on the integral of C_v vs T is very small (<1 J mol^{-1}) and well within the uncertainties quoted for $\Delta_f H^{\ominus}_{298.15}$ (C_2H_5) above. Fig 6 also shows a plot of C_v/R vs T based on the energy levels obtained by Kreglewski and Gulaczyk.[54] The agreement is excellent, confirming the validity of our hindered rotor model.

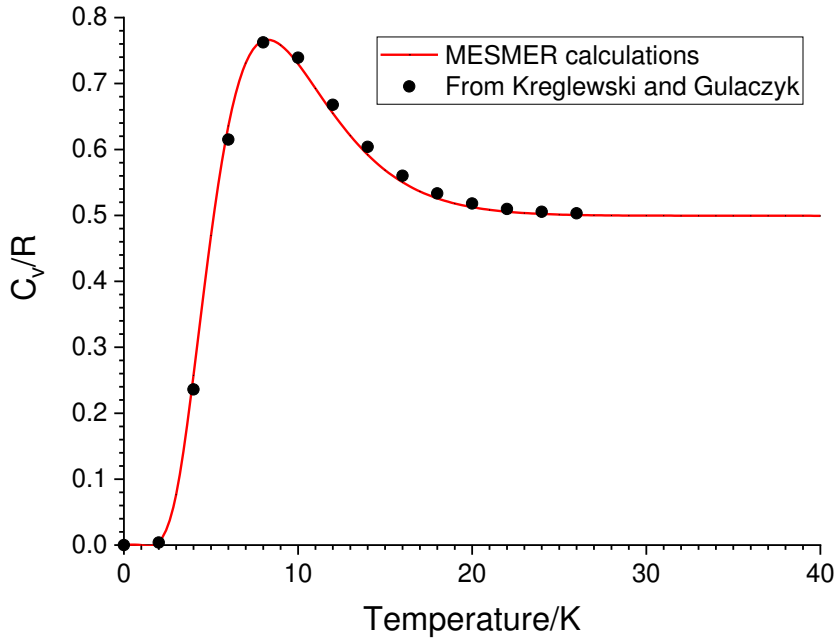

Figure 6. Plot of C_v/R as a function of temperature based on the *ab initio* potential calculated in this work (solid red line). The value approaches the classical limit (C_v/R = 0.5) by ~23 K. The figure also shows values calculated from the energy levels given by Kreglewski and Gulaczyk (black circles).[54] The inversion mode makes a negligible contribution to C_v at these temperatures.

5.2.2 Activation Threshold and Imaginary Frequency

Table 6 shows that the PES parameters derived from the He data vary by very small amounts when data from other bath gases are introduced: the threshold for the association reaction is lowered slightly, but after rounding remains effectively the same and υ_{imag} is slightly larger but, again, with rounding remains unchanged. The value of υ_{imag} does depend on the model adopted for tunnelling. The value obtained from *ab initio* calculations is 1103 cm^{-1} which is clearly significantly different from the value obtained from the fit. Miller and Klippenstein[28] quote *ab initio* values of υ_{imag} ranging from 335 cm^{-1} to 900 cm^{-1}. The best value, 765 cm^{-1}, which was used in an Eckart model of tunneling in the FTST calculations performed by Miller and Klippenstein, clearly falls within the error bars of the fitted value of this parameter.

The results of this work are of course dependent on the model used. We have investigated the role of the torsion and low frequency inversion. As long as the torsion is treated as a hindered rotor (and indeed, because of the low barrier of ~20 cm^{-1}, it can be treated as a free rotor for most temperatures), the fit to the experimental data produces well defined thermodynamic parameters that are in good agreement with our *ab initio* calculations and the ATcT values. Other model

parameters that are varied in the fit to experimental data include the reaction threshold energy, the imaginary frequency, incorporated in an Eckart tunneling model and bath-gas dependent parameters in an exponential down model for energy transfer. These are common parameters used in a variety of models. The good agreement for the enthalpy of formation of ethyl between our fixed transition state model and the ILT model suggests that, because of the wide range of conditions of our fitting, the enthalpy of reaction is relatively insensitive to tunneling. The use of alternative, more sophisticated, energy transfer models or a 2-D master equation may slightly alter the results obtained from the fitting process, but the effects on the ethyl enthalpy of formation would likely be small.

5.3 Rate Coefficients

5.3.1 Limiting High Pressure Rate Coefficient, $k_1^\infty(T)$

The best fit parameters, ΔE_{thresh}= 11.43 kJ mol^{-1} and υ_{imag} = 731 cm^{-1} (Table 6), were combined with the calculated frequencies for the reactants and the transition state (see SI, Table S3), an Eckart model for tunnelling, and a constrained transition state or an ILT approach, to give:

$k_1^\infty(T) = 7.04\text{x}10^{-12}(T/300\text{ K})^{1.971}\exp(-1030\text{ K}/T)$ cm^3 molecule^{-1} s^{-1}. (TS MODEL)

$k_1^\infty(T) = 1.33\text{x}10^{-11}(T/300\text{ K})^{1.438}\exp(-1433\text{ K}/T)$ cm^3 molecule^{-1} s^{-1}. (ILT MODEL)

Using a variational model, Miller and Klippenstein[28] obtained

$k_1^\infty(T) = 9.55\text{x}10^{-12}(T/300\text{ K})^{1.463}\exp(-1355\text{ K}/T)$ cm^3 molecule^{-1} s^{-1}.

These rate coefficients are compared in Figure 7 over the temperature range 200 – 1500 K. The values from the fixed transition state model expression determined here exceed those of Miller and Klippenstein by 50% at 800 K. A component of this difference presumably arises from the effects of rotation that are imperfectly captured in the constrained transition state model, but the difference is also due to the lower threshold from our fitted data compared to the calculated value of Miller and Klippenstein. Our ILT model falls below the fixed TS model at higher temperatures, reflecting the variational nature of the TS, but our ILT model (again based on the fit to experiment) is 19% faster at 800 K compared to Miller and Klippenstein.

The limiting high pressure rate coefficient for dissociation, obtained from the best fit model is:

$k_{-1}^\infty(T) = 1.40\text{x}10^{12}(T/300\text{ K})^{2.257}\exp(-36020\text{ K}/T)$ s^{-1}

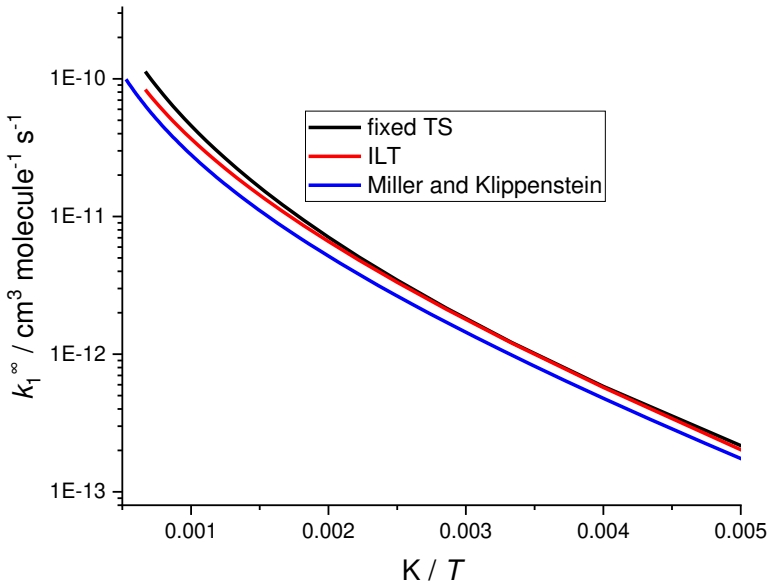

Figure 7. Variation of $k_1^{\infty}(T)$ vs temperature using a fixed transition state with the parameters derived from the optimized fitting of the experimental data (black line), using the ILT parameters (red line) and from the calculations of Miller and Klippenstein (blue line).[28]

5.3.2 Pressure Dependent Rate Coefficients and Implications for Combustion

Troe parameters were obtained from fitting to association and dissociation data obtained from master equation calculations based on our best-fit parameters using helium, see Table 4, in the temperature range, 300 < T/K < 1500 and gas density range, 10^{15} < [He]/molecule cm^{-3} < 10^{25}. The Troe expression used is given in Troe and Ushakov.[78] The best fit parameter values for k_1 are given in the final column of Table 8. The equation used to parameterize the master equation data is shown in Section 9 of the SI. k_1, k_{-1} and equilibrium constant data are tabulated in Tables S10 and S11. The dissociation data for k_{-1} were calculated from k_1 via the equilibrium constant K_p and Table S12 gives the NASA polynomials to calculate the equilibrium constant. The fit to the data is better than 10% on average and the biggest deviation is about 20%. The fits were restricted to T > 300 K because deviations from the fit increased considerably below this temperature. Miller and Klippenstein[28] noted that, "the expressions for k_1^0 are not the true low-pressure limit rate coefficients; they are simply fitting parameters." The same applies to the values determined here.

Table 8. MESMER fitted parameters for k_1 together with literature data, and the Troe fitting parameters to the MESMER simulations using N_2 as the buffer gas. The high and low pressure limits is given in the form: $k_1(T) = A\,(T/300)^n \exp(-Ea_1/RT)$ cm^3 molecule^{-1} s^{-1}.

	Troe parameters[79] from Miller and Klippenstein[28]	Troe parameters this work[78]
$\langle \Delta E \rangle_{d,298}$(He) / cm^{-1}	75×(T/300 K)$^{0.95}$	47.5×(T/298 K)$^{1.28}$
A_1^{∞} / cm^3 s^{-1}	9.55 x 10^{-12}	8.62 × 10^{-12}
n^{∞}	1.46	1.87
Ea_1^{∞} / J mol^{-1}	5670	4876
A_1^0 / cm^6 molecule^{-2} s^{-1}	1.97 x 10^{-25}	6.80 × 10^{-23}
n^0	-6.64	-6.20
Ea_1^0 / J mol^{-1}	24140	19910
Fc	1.569e$^{(-T/299)}$-0.569e$^{(T/9147)}$ +e$^{(-152.4/T)}$	
b		0.483
x_0		1.163
F_{cent}A		0.00176
$F_{cent}B$		3.38 × 10^{-4}

Figure 8 shows a plot of the apparent value of k_1^0 vs T for He as the bath gas. These values were determined from the master equation calculations, at a series of decreasing values of [M], assuming that the low pressure limit had been reached at each [M]. The apparent k_1^0 increases as [M] decreases to 1x10^5 molecule cm^{-3}, showing convergence at the lower pressures. The values at [M] = 1x10^5 molecule cm^{-3} were used to determine k_1^0:

$k_1^0(T)$ = 2.41 x 10^{-23}(T/300)$^{-5.64}$ exp(-17044/RT) cm^6 molecule^{-2} s^{-1}

The k_1^0 values obtained by Miller and Klippenstein, which are also shown in Figure 8, are greater, especially at low T. This problem was noted by Miller and Klippenstein in their comparison with the results of Feng et al.[17] and Lightfoot and Pilling.[61] They attributed the discrepancy to the omission of tunnelling at the low-pressure limit in the earlier analyses. They commented that "at the low pressure limit the barriers are transparent" and failure to incorporate tunnelling significantly underestimates the rate constant. Tunnelling was included in our model, but the results indicate that basing the determination of k_1^0 on an extrapolation from higher pressures may still underestimate the effects of tunnelling.

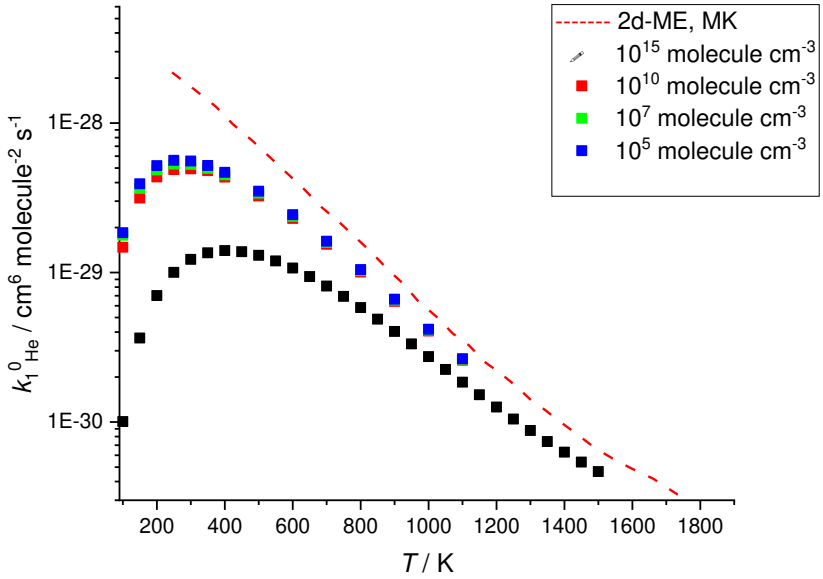

Figure 8. The approach to the low-pressure limit of the association reaction as a function of temperature and comparison with Miller and Klippenstein.[28]

The main competing reactions for the ethyl radical in combustion systems are dissociation and reaction with O_2. Under low temperature combustion conditions, the latter leads to peroxy radical formation and is much faster than ethyl dissociation for typical [O_2]. At higher temperatures, the peroxy radical dissociates rapidly and the reaction with O_2 becomes

$$C_2H_5 + O_2 \rightarrow C_2H_4 + HO_2 \qquad \text{(R3)}$$

Miller and Klippenstein[80] calculated k_3 using a master equation model. Figure 9 compares k_{-1} and $k_3[O_2]$ in He with a total bath gas concentration of 10^{19} molecule cm^{-3} and with [O_2] = 2 x 10^{18} molecule cm^{-3}. Reaction R3 dominates at temperatures below ~1000 K and R-1 above ~1400 K. These conclusions are little changed for combustion in air. k_{-1} may increase slightly in N_2 compared with He. k_{-1} also increases with pressure, but in air $k_{-1}[O_2]$ would, of course, scale linearly with total pressure.

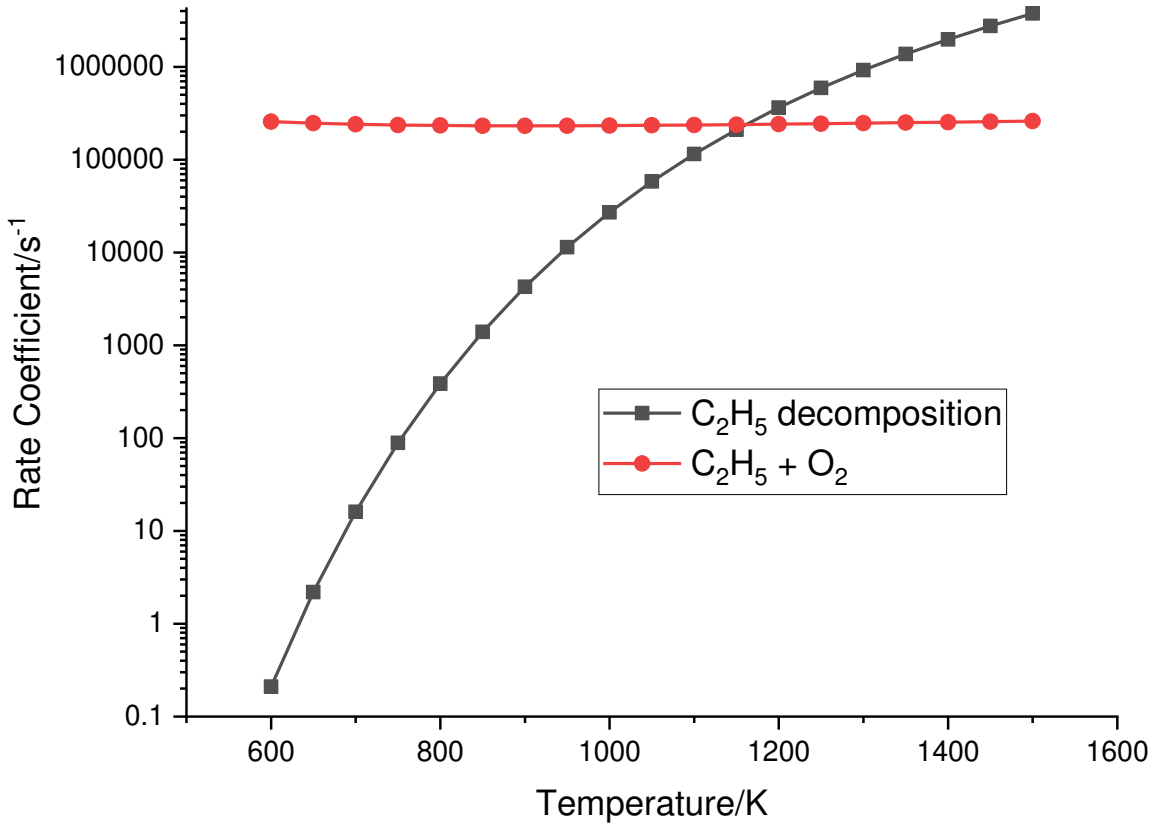

Figure 9. Comparison of rate coefficient for C_2H_5 decomposition (k_{-1}) versus pseudo-first order rate coefficient for the reaction of C_2H_5 with oxygen ($[O_2]$ = 2 x 10^{18} molecule cm^{-3}) with a helium bath gas at 1 x 10^{19} molecule cm^{-3}. Under these conditions the rate coefficients are equal at a temperature of ~1150 K.

5.3.3 Energy Transfer

The experiments discussed in Section 2 were undertaken because of the discrepancy in energy transfer parameters observed by Feng et al.[17] between their results and the results of Brouard et al.[10] and Hanning-Lee et al.[11] The present analysis reveals no such discrepancy. The scatter of the latter results, obtained at higher pressures and under equilibration conditions, are significantly greater than those obtained by Feng et al. (Figure 4). Nevertheless, there is no evidence of bias or systematic effects. The reduced residuals from the analysis of the data of Feng et al. lie around and close to the zero line, but they do show a systematic increase with increasing pressure. This may reflect an inadequacy of the simple energy transfer model employed in the ME calculations, that is not revealed in the other studies, because of the greater scatter in those data compared to the data of Feng et al.

It proved difficult to obtain fits for the energy transfer parameters for ethane because of systematic variations of the reduced residuals with pressure for the datasets of Simon et al.[70] and Loucks and

Laidler.[67] The origin of these variations is unclear. The final recommendations are based only on the data of Lin and Back[66] and of Pacey and Wimalasena.[68]

The values of $\langle \Delta E \rangle_d$ for the other bath gases are based on the low pressure measurements of Michael et al.[63] at 300 K. Analysis of the low temperature data of Lee et al.[71] showed good agreement at 300 K, but with an unexpected negative temperature dependence. The data of Sugawara et al. [72] in H_2 are inconsistent with the measurements of Michael et al. but, since they are close to the high-pressure limit, they are relatively insensitive to $\langle \Delta E \rangle_d$.

6. Conclusions

The primary goal of this work has been to determine the heat of formation of the ethyl radical. Results of the experimental determination of the rate coefficient for the association reaction have also been presented. These data have been combined with existing experimental data and analysed to determine the value of heat of formation of the ethyl radical. A strength of the current approach is that, for the first time, we combine data from a wide range of conditions, bath gases and experimental techniques. The fitting of experimental data is a significant difference from the earlier study of Miller and Klippenstein.[28] which *compares* theoretical and experimental results. In the present study, theory plays a key role in limiting the number of variable parameters (e.g. through the calculation of molecular properties), and in providing initial estimates of parameters such as $\Delta_r H_0^{\ominus}$ and ΔE_{thresh} that are varied in the fit. The strength of the method, though, is the use of the MESMER code to provide a global fit to the large amount of experimental data.

The analysis also allowed a number of conclusions to be drawn, which are now summarized:

a. Using the complete hindered rotor treatment in the master equation, the value obtained from the data fitting for $\Delta_r H_0^{\ominus}$ is in good agreement with the values obtained from *ab initio* calculations in this work and by Miller and Klippenstein.[28] Using enthalpies of formation for H and C_2H_4 from the Active Thermochemical Tables, gives $\Delta_f H_0^{\ominus}(C_2H_5)$= 131.55 ± 0.57 kJ mol^{-1}, in good agreement with the ATcT value of 131.04 ± 0.27 kJ mol^{-1}(the quoted uncertainties are ± 2 standard deviations in both cases)
b. The new experimental data set obtained as part of this work is consistent with previous experimental work under similar conditions. In addition, for the He bath gas case, the present master equation fitting analysis, using more data and analysing both association and dissociation data simultaneously, does not indicate any significant inconsistency between data sets as has been suggested in an earlier analysis.[17]
c. A key quantity in the present analysis was the density of states of the ethyl radical. The internal rotor mode and the inversion mode at the radical centre were singled out for a particular attention as these modes are anharmonic and have large amplitudes. The densities of states associated with these modes were calculated in a number of ways and corresponding fits were done. For the internal rotation mode, it is clear from these fits, that an accurate solution to the corresponding Schrödinger equation for this mode gave the best agreement with the literature value for $\Delta_f H_0^{\ominus}(C_2H_5)$ and this is in alignment with the general view of these types of mode. For the inversion mode the case is less clear cut;

none-the-less an accurate one-dimensional solution for this mode is relatively straightforward and should be used in any future analysis.

d. The values of $\Delta_r H_0^{\ominus}$ returned from ILT and RRKM with tunnelling analyses were found to be very similar. The value obtained for the reaction threshold for reaction (R1) from the fit based on RRKM theory with tunnelling and from *ab initio* theory are also very similar. The, approximately, equivalent parameter from an ILT analysis, ΔE_{act}, is significantly smaller and it is speculated that this difference reflects the effect of tunnelling on the data fitting for adjustments for the ILT approach.
e. The determination of the energy transfer parameters of ethane as a bath gas were problematic because the ethane datasets appear to be incompatible with each other as shown by skewed residuals. Attempts at fitting all the ethane bath gas data simultaneously gave a poor fit with unrealistic parameters. It appears that systematic errors exist in some data sets that render the sets incompatible. Determining which sets have the largest such errors is somewhat subjective; however, it was shown that removal of some data sets leads to more realistic and consistent parameters.
f. Our final recommendation of the PES parameters is based on the fit of He bath gas data, selected ethane data and Ar and H_2 measurements which includes low temperature data, which help constrain the barrier and imaginary frequency. However, there is little variation in the PES parameters compared to the helium only fits (Table 6).
g. The divergence of the best fit k_1^{∞} at high temperatures from the variational model of Miller and Klippenstein[28] suggests variational effects play a small role at high energies.

Supplementary Information

Supplementary information associated with this paper contains information on global analysis, experimental details (Table S1), *ab initio* calculations at various levels of theory (Table S2) and resultant frequencies (Table S3), table of helium bath gas data used in the analysis (Table S4), table of ethane bath gas data used in the analysis (Table S5), results from considering the combination of individual ethane datasets with the helium bath gas dataset (Table S6), thermodynamic data for ethyl, ethene and H (Tables S7 – 9), equation used for Troe parameterization of the master equation data, tabulations of k_1, k_{-1}, K (Tables S10 and S11), NASA polynomials for enthalpy and entropy of reaction (Table S12) and an example MESMER file for data fitting.

Acknowledgements

We are grateful to the NERC National Centre for Atmospheric Science for funding for MAB and to the NERC Doctoral Training Programme for funding for THS.

References

1. Ruscic, B.; Pinzon, R. E.; Morton, M. L.; von Laszevski, G.; Bittner, S. J.; Nijsure, S. G.; Amin, K. A.; Minkoff, M.; Wagner, A. F., Introduction to active thermochemical tables: Several "key" enthalpies of formation revisited. *J. Phys. Chem. A* **2004,** *108* (45), 9979-9997.

2. Ruscic, B.; Bross, D. H. Active thermochemical tables (atct) values based on ver. 1.122p of the thermochemical network (2020);. https://atct.anl.gov/Thermochemical%20Data/version%201.122p/index.php.
3. Klippenstein, S. J.; Harding, L. B.; Ruscic, B., Ab Initio computations and active thermochemical tables hand in hand: Heats of formation of core combustion species. *J. Phys. Chem. A* **2017,** *121* (35), 6580-6602.
4. Ruscic, B.; Berkowitz, J.; Curtiss, L. A.; Pople, J. A., The ethyl radical - photoionization and theoretical-studies. *J. Chem. Phys.* **1989,** *91* (1), 114-121.
5. Lau, K. C.; Ng, C. Y., Accurate ab initio predictions of ionization energies of hydrocarbon radicals: CH_2, CH_3, C_2H, C_2H_3, C_2H_5, C_3H_3, and C_3H_5. *J. Chem. Phys.* **2005,** *122* (22), 9.
6. King, K. D.; Golden, D. M.; Benson, S. W., Absolute rate constants and arrhenius parameters for reaction of bromine atoms with ethane. *Transactions of the Faraday Society* **1970,** *66* (575), 2794-2798.
7. Nicovich, J. M.; Vandijk, C. A.; Kreutter, K. D.; Wine, P. H., Kinetics of the reactions of alkyl radicals with HBr and DBr. *J. Phys. Chem.* **1991,** *95* (24), 9890-9896.
8. Seakins, P. W.; Pilling, M. J.; Niiranen, J. T.; Gutman, D.; Krasnoperov, L. N., Kinetics and thermochemistry of R+HBr = RH+Br reactions - determinations of the heat of formation of C_2H_5, i-C_3H_7, sec-C_4H_9, and t-C_4H_9. *J. Phys. Chem.* **1992,** *96* (24), 9847-9855.
9. Dobis, O.; Benson, S. W., Temperature coefficients of rates of ethyl radical reactions with HBr and Br in the 228-368 K temperature range at millitorr pressures. *J. Phys. Chem. A* **1997,** *101* (34), 6030-6042.
10. Brouard, M.; Lightfoot, P. D.; Pilling, M. J., Observation of equilibration in the system H + C_2H_4 = C_2H_5 - the determination of the heat of formation of C_2H_5. *J. Phys. Chem.* **1986,** *90* (3), 445-450.
11. Hanninglee, M. A.; Green, N. J. B.; Pilling, M. J.; Robertson, S. H., Direct observation of equilibration in the system H+C_2H_4 = C_2H_5 - standard enthalpy of formation of the ethyl radical. *J. Phys. Chem.* **1993,** *97* (4), 860-870.
12. Glowacki, D. R.; Liang, C. H.; Morley, C.; Pilling, M. J.; Robertson, S. H., Mesmer: An open-source master equation solver for multi-energy well reactions. *J. Phys. Chem. A* **2012,** *116* (38), 9545-9560.
13. Barker, J. R., Multiple-well, multiple-path unimolecular reaction systems. I. Multiwell computer program suite. *Int. J. Chem. Kinet.* **2001,** *33* (4), 232-245.
14. Georgievskii, Y.; Miller, J. A.; Burke, M. P.; Klippenstein, S. J., Reformulation and solution of the master equation for multiple-well chemical reactions. *J. Phys. Chem. A* **2013,** *117* (46), 12146-12154.
15. McKee, K.; Blitz, M. A.; Pilling, M. J., Temperature and pressure studies of the reactions of CH_3O_2, HO_2, and 1,2-$C_4H_9O_2$ with NO_2. *J. Phys. Chem. A* **2016,** *120* (9), 1408-1420.
16. Medeiros, D. J.; Robertson, S. H.; Blitz, M. A.; Seakins, P. W., Direct trace fitting of experimental data using the master equation: Testing theory and experiments on the OH + C_2H_4 reaction. *J. Phys. Chem. A* **2020,** *124* (20), 4015-4024.
17. Feng, Y.; Niiranen, J. T.; Bencsura, A.; Knyazev, V. D.; Gutman, D.; Tsang, W., Weak collision effects in the reaction C_2H_5 = C_2H_4+H. *J. Phys. Chem.* **1993,** *97* (4), 871-880.
18. Gannon, K. L.; Blitz, M. A.; Pilling, M. J.; Seakins, P. W.; Klippenstein, S. J.; Harding, L. B., Kinetics and product branching ratios of the reaction of $^1CH_2$ with H_2 and D_2. *J. Phys. Chem. A* **2008,** *112* (39), 9575-9583.
19. Gannon, K. L.; Glowacki, D. R.; Blitz, M. A.; Hughes, K. J.; Pilling, M. J.; Seakins, P. W., H atom yields from the reactions of CN radicals with C_2H_2, C_2H_4, C_3H_6, trans-2-C_4H_8, and iso-C_4H_8. *J. Phys. Chem. A* **2007,** *111* (29), 6679-6692.
20. Kovacs, T.; Blitz, M. A.; Seakins, P. W., H-atom yields from the photolysis of acetylene and from the reaction of C_2H with H_2, C_2H_2, and C_2H_4. *J. Phys. Chem. A* **2010,** *114* (14), 4735-4741.
21. Kovacs, T.; Blitz, M. A.; Seakins, P. W.; Pilling, M. J., H atom formation from benzene and toluene photoexcitation at 248 nm. *J. Chem. Phys.* **2009,** *131* (20).
22. Keller-Rudek, H.; Moortgat, G. K.; Sander, R.; Sorensen, R., The MPI-Mainz UV/vis spectral atlas of gaseous molecules of atmospheric interest. *Earth Syst. Sci. Data* **2013,** *5* (2), 365-373.
23. Mahon, R.; McIlrath, T. J.; Myerscough, V. P.; Koopman, D. W., 3rd-harmonic generation in argon, krypton, and xenon - bandwidth limitations in the vicinity of lyman-alpha. *IEEE J. Quantum Electron.* **1979,** *15* (6), 444-451.

24. Okabe, H., Intense resonance line sources for photochemical work in vacuum ultraviolet region. *Journal of the Optical Society of America* **1964,** *54* (4), 478-&.
25. Fahr, A.; Tardy, D. C., Rate coefficients and products of ethyl and vinyl cross-radical reactions. *J. Phys. Chem. A* **2002,** *106* (46), 11135-11140.
26. Robertson, S. H., Foundations of the master equation. *Comprehensive Chemical Kinetics* **2019,** *43*, 291-361.
27. Miller, J. A.; Sivaramakrishnan, R.; Tao, Y. J.; Goldsmith, C. F.; Burke, M. P.; Jasper, A. W.; Hansen, N.; Labbe, N. J.; Glarborg, P.; Zador, J., Combustion chemistry in the twenty-first century: Developing theory-informed chemical kinetics models. *Prog. Energy Combust. Sci.* **2021,** *83*, 53.
28. Miller, J. A.; Klippenstein, S. J., The H+C_2H_2 (+M) = C_2H_3 (+M) and H+C_2H_4 (+M) = C_2H_5 (+M) reactions: Electronic structure, variational transition-state theory, and solutions to a two-dimensional master equation. *PCCP* **2004,** *6* (6), 1192-1202.
29. Frisch, M. J.; Trucks, G. W.; Schlegel, H. B.; Scuseria, G. E.; Robb, M. A.; Cheeseman, J. R.; Scalmani, G.; Barone, V.; Petersson, G. A.; Nakatsuji, H., et al. *Gaussian 09, revision a.02*, Gaussian: Wallingford CT, 2009.
30. Johnson, R., Nist 101 computational chemistry comparison and benchmark database. NIST: Gaithersburg MD, 1999.
31. Barone, V., Anharmonic vibrational properties by a fully automated second-order perturbative approach. *J. Chem. Phys.* **2005,** *122* (1), 014108.
32. Hratchian, H. P.; Schlegel, H. B., Accurate reaction paths using a hessian based predictor-corrector integrator. *J. Chem. Phys.* **2004,** *120* (21), 9918-9924.
33. Peterson, K. A.; Woon, D. E.; Dunning, T. H., Benchmark calculations with correlated molecular wave-functions .4. The classical barrier height of the H+H_2 -> H_2+H reaction. *J. Chem. Phys.* **1994,** *100* (10), 7410-7415.
34. Woon, D. E.; Dunning, T. H., Benchmark calculations with correlated molecular wave-functions .6. Second row A_2 and first row second row AB diatomic-molecules. *J. Chem. Phys.* **1994,** *101* (10), 8877-8893.
35. Feller, D.; Peterson, K. A.; Hill, J. G., On the effectiveness of CCSD(T) complete basis set extrapolations for atomization energies. *J. Chem. Phys.* **2011,** *135* (4).
36. Mebel, A. M.; Morokuma, K.; Lin, M. C., Ab-initio molecular-orbital study of potential-energy surface for the reaction of C_2H_3 with H_2 and related reactions. *J. Chem. Phys.* **1995,** *103* (9), 3440-3449.
37. Hase, W. L.; Schlegel, H. B.; Balbyshev, V.; Page, M., An ab initio study of the transition state and forward and reverse rate constants for C_2H_5 = H+C_2H_4. *J. Phys. Chem.* **1996,** *100* (13), 5354-5361.
38. Villa, J.; Gonzalez-Lafont, A.; Lluch, J. M.; Truhlar, D. G., Entropic effects on the dynamical bottleneck location and tunneling contributions for C_2H_4+H -> C_2H_5: Variable scaling of external correlation energy for association reactions. *J. Am. Chem. Soc.* **1998,** *120* (22), 5559-5567.
39. Villa, J.; Corchado, J. C.; Gonzalez-Lafont, A.; Lluch, J. M.; Truhlar, D. G., Variational transition-state theory with optimized orientation of the dividing surface and semiclassical tunneling calculations for deuterium and muonium kinetic isotope effects in the free radical association reaction H+C_2H_4 -> C_2H_5. *J. Phys. Chem. A* **1999,** *103* (26), 5061-5074.
40. Werner, H. J.; Knowles, P. J.; Knizia, G.; Manby, F. R.; Schutz, M., Molpro: A general-purpose quantum chemistry program package. *Wiley Interdiscip. Rev.-Comput. Mol. Sci.* **2012,** *2* (2), 242-253.
41. Wu, J. J.; Gao, L. G.; Ren, W.; Truhlar, D. G., Anharmonic kinetics of the cyclopentane reaction with hydroxyl radical. *Chem. Sci.* **2020,** *11* (9), 2511-2523.
42. Barker, J. R., Sums of quantum states for nonseparable degrees of freedom - multidimensional Monte-Carlo integration. *J. Phys. Chem.* **1987,** *91* (14), 3849-3854.
43. Barker, J. R.; Stanton, J. F.; Nguyen, T. L., Semiclassical transition state theory/master equation kinetics of ho plus co: Performance evaluation. *Int. J. Chem. Kinet.* **2020,** *52* (12), 1022-1045.
44. Pitzer, K. S.; Gwinn, W. D., Energy levels and thermodynamic functions for molecules with internal rotation i rigid frame with attached tops. *J. Chem. Phys.* **1942,** *10* (7), 428-440.
45. Gang, J.; Pilling, M. J.; Robertson, S. H., Monte Carlo calculation of partition functions for straight chain alkanes. *Chem. Phys.* **1998,** *231* (2-3), 183-192.

46. Allinger, N. L., Conformational-analysis MM2 - hydrocarbon force-field utilizing V1 and V2 torsional terms. *J. Am. Chem. Soc.* **1977,** *99* (25), 8127-8134.
47. Allinger, N. L.; Yuh, Y. H.; Lii, J. H., Molecular mechanics - the MM3 force-field for hydrocarbons .1. *J. Am. Chem. Soc.* **1989,** *111* (23), 8551-8566.
48. Bao, J. L.; Xing, L. L.; Truhlar, D. G., Dual-level method for estimating multistructural partition functions with torsional anharmonicity. *Journal of Chemical Theory and Computation* **2017,** *13* (6), 2511-2522.
49. Simon-Carballido, L.; Bao, J. L.; Alves, T. V.; Meana-Paneda, R.; Truhlar, D. G.; Fernandez-Ramos, A., Anharmonicity of coupled torsions: The extended two-dimensional torsion method and its use to assess more approximate methods. *Journal of Chemical Theory and Computation* **2017,** *13* (8), 3478-3492.
50. Miller, T. F.; Clary, D. C., Torsional path integral Monte Carlo method for the quantum simulation of large molecules. *J. Chem. Phys.* **2002,** *116* (19), 8262-8269.
51. Miller, T. F.; Clary, D. C., Torsional anharmonicity in the conformational thermodynamics of flexible molecules. *Mol. Phys.* **2005,** *103* (11-12), 1573-1578.
52. Sturdy, Y. K.; Clary, D. C., Torsional anharmonicity in transition state theory calculations. *PCCP* **2007,** *9* (19), 2397-2405.
53. Beyer, T.; Swinehart, D. F., Number of multiply-restricted partitions. *Communications of the Acm* **1973,** *16* (6), 379-379.
54. Kreglewski, M.; Gulaczyk, I., Inversion-torsional motion in the ethyl radical. *Chem. Phys. Lett.* **2014,** *592*, 307-313.
55. Bross, D. H.; Yu, H. G.; Harding, L. B.; Ruscic, B., Active thermochemical tables: The partition function of hydroxymethyl (CH_2OH) revisited. *J. Phys. Chem. A* **2019,** *123* (19), 4212-4231.
56. Stare, J.; Balint-Kurti, G. G., Fourier grid hamiltonian method for solving the vibrational schrodinger equation in internal coordinates: Theory and test applications. *J. Phys. Chem. A* **2003,** *107* (37), 7204-7214.
57. Miller, W. H., Tunneling corrections to unimolecular rate constants, with application to formaldehyde. *J. Am. Chem. Soc.* **1979,** *101* (23), 6810-6814.
58. Senosiain, J. P.; Klippenstein, S. J.; Miller, J. A., Reaction of ethylene with hydroxyl radicals: A theoretical study. *J. Phys. Chem. A* **2006,** *110* (21), 6960-6970.
59. Press, W. H.; Teukolsky, S. A.; Vitterling, W. T.; Flannery, B. P., *Numerical recipes in c++*. Cambridge University Press: Cambridge, 2002.
60. Bevington, P. R. S., *Data reduction and error analysis for the physical sciences*. McGraw-Hill: New York, 1969.
61. Lightfoot, P. D.; Pilling, M. J., Temperature and pressure-dependence of the rate-constant for the addition of H to C_2H_4. *J. Phys. Chem.* **1987,** *91*, 3373.
62. Kurylo, M. J.; Peterson, N. C.; Braun, W., Absolute rates of reactions $H+C_2H_4$ and $H+C_2H_5$. *J. Chem. Phys.* **1970,** *53* (7), 2776-&.
63. Michael, J. V.; Osborne, D. T.; Suess, G. N., Reaction $H+C_2H_4$ - investigation into effects of pressure, stoichiometry, and nature of third body species. *J. Chem. Phys.* **1973,** *58* (7), 2800-2806.
64. Barker, J. R.; Michael, J. V., Reaction of hydrogen atoms with ethylene. *J. Chem. Phys.* **1969,** *51* (2), 850-&.
65. Barker, J. R.; Keil, D. G.; Michael, J. V.; Osborne, D. T., Reaction $H+C_2H_4$ - comparison of three experimental techniques. *J. Chem. Phys.* **1970,** *52* (4), 2079-&.
66. Lin, M. C.; Back, M. H., Thermal decomposition of ethane .2. Unimolecular decomposition of ethane molecule and ethyl radical. *Can. J. Chem.* **1966,** *44* (20), 2357-&.
67. Loucks, L. F.; Laidler, K. J., Thermal decomposition of ethyl radical. *Can. J. Chem.* **1967,** *45* (22), 2795-&.
68. Pacey, P. D.; Wimalasena, J. H., Kinetics and thermochemistry of the ethyl radical - the induction period in the pyrolysis of ethane. *J. Phys. Chem.* **1984,** *88* (23), 5657-5660.
69. Trenwith, A. B., The pyrolysis of ethane - a study of the dissociation reaction C_2H_5- C_2H_4+H. *Journal of the Chemical Society-Faraday Transactions II* **1986,** *82*, 457-463.

70. Simon, Y.; Foucaut, J. F.; Scacchi, G., Experimental study and theoretical modeling of thermal decomposition of the ethyl radical. *Canadian Journal of Chemistry-Revue Canadienne De Chimie* **1988,** *66* (9), 2142-2150.
71. Lee, J. H.; Michael, J. V.; Payne, W. A.; Stief, L. J., Absolute rate of reaction of atomic-hydrogen with ethylene from 198 to 320 K at high-pressure. *J. Chem. Phys.* **1978,** *68* (4), 1817-1820.
72. Sugawara, K. I.; Okazaki, K.; Sato, S., Temperature-dependence of the rate constants of H and D-atom additions to C_2H_4, C_2H_3D, C_2D_4, C_2H_2, and C_2D_2. *Bull. Chem. Soc. Jpn.* **1981,** *54* (10), 2872-2877.
73. Sears, T. J.; Johnson, P. M.; Jin, P.; Oatis, S., Infrared laser transient absorption spectroscopy of the ethyl radical. *J. Chem. Phys.* **1996,** *104* (3), 781-792.
74. Davies, J. W.; Green, N. J. B.; Pilling, M. J., The testing of models for unimolecular decomposition via inverse laplace transformation of experimental recombination data. *Chem. Phys. Lett.* **1986,** *126*, 373.
75. Jasper, A. W., "Third-body" collision parameters for hydrocarbons, alcohols, and hydroperoxides and an effective internal rotor approach for estimating them. *Int. J. Chem. Kinet.* **2020,** *52* (6), 387-402.
76. Jasper, A. W., Microcanonical rate constants for unimolecular reactions in the low-pressure limit. *J. Phys. Chem. A* **2020,** *124* (7), 1205-1226.
77. Lin, M. C.; Laidler, K. J., Theory of unimolecular decomposition of ethane and of ethyl and methoxymethyl radicals. *Transactions of the Faraday Society* **1968,** *64* (541P), 79-&.
78. Troe, J.; Ushakov, V. G., Representation of "broad" falloff curves for dissociation and recombination reactions. *Zeitschrift Fur Physikalische Chemie-International Journal of Research in Physical Chemistry & Chemical Physics* **2014,** *228* (1), 1-10.
79. Gilbert, R. G.; Luther, K.; Troe, J., Theory of thermal unimolecular reactions in the fall-off range .2. Weak collision rate constants. *Ber. Bunsen-Ges. Phys. Chem. Chem. Phys.* **1983,** *87* (2), 169-177.
80. Miller, J. A.; Klippenstein, S. J., The reaction between ethyl and molecular oxygen ii: Further analysis. *Int. J. Chem. Kinet.* **2001,** *33* (11), 654-668.

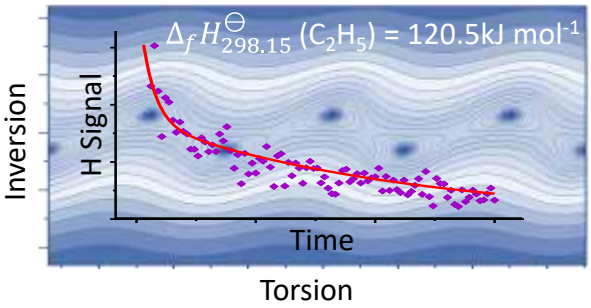
$\Delta_f H^{\ominus}_{298.15}$ (C_2H_5) = 120.5kJ mol^{-1}
H Signal
Time
Inversion
Torsion